remote sensing

MDPI

Article

Advanced Semi-Automatic Approach for Identifying Damaged Surfaces in Cultural Heritage Sites: Integrating UAVs, Photogrammetry, and 3D Data Analysis

Tudor Caciora [1,*], Alexandru Ilieș [1], Grigore Vasile Herman [1], Zharas Berdenov [2], Bahodirhon Safarov [3], Bahadur Bilalov [4], Dorina Camelia Ilieș [1], Ștefan Baias [1] and Thowayeb H. Hassan [5,6]

[1] Department of Geography, Tourism and Territorial Planning, Faculty of Geography, Tourism and Sport, University of Oradea, 1 Universitatii Street, 410087 Oradea, Romania; ilies@uoradea.ro (A.I.); gherman@uoradea.ro (G.V.H.); dilies@uoradea.ro (D.C.I.); sbaias@uoradea.ro (Ș.B.)
[2] Faculty of Science, L.N. Gumilyov Eurasian National University, 2 Satpayev Street, Nur-Sultan 010008, Kazakhstan; berdenov-z@mail.ru
[3] Department of Digital Economy, Samarkand State University, Samarkand 140105, Uzbekistan; safarovb@rambler.ru
[4] Department of Tourism Business, Azerbaijan University of Tourism and Management, Baku 1172, Azerbaijan; b.bilalov@atmu.edu.az
[5] Social Studies Department, College of Arts, King Faisal University, Al Ahsa 31982, Saudi Arabia; thassan@kfu.edu.sa
[6] Tourism Studies Department, Faculty of Tourism and Hotel Management, Helwan University, Cairo 12612, Egypt
* Correspondence: tudor.caciora@uoradea.ro; Tel.: +40-740941144

Abstract: The analysis and preservation of the cultural heritage sites are critical for maintaining their historical and architectural integrity, as they can be damaged by various factors, including climatic, geological, geomorphological, and human actions. Based on this, the present study proposes a semi-automatic and non-learning-based method for detecting degraded surfaces within cultural heritage sites by integrating UAV, photogrammetry, and 3D data analysis. A 20th-century fortification from Romania was chosen as the case study due to its physical characteristics and state of degradation, making it ideal for testing the methodology. Images were collected using UAV and terrestrial sensors and processed to create a detailed 3D point cloud of the site. The developed pipeline effectively identified degraded areas, including cracks and material loss, with high accuracy. The classification and segmentation algorithms, including K-means clustering, geometrical features, RANSAC, and FACETS, improved the detection of destructured areas. The combined use of these algorithms facilitated a detailed assessment of the structural condition. This integrated approach demonstrated that the algorithms have the potential to support each other in minimizing individual limitations and accurately identifying degraded surfaces. Even though some limitations were observed, such as the potential for the overestimation of false negatives and positives areas, the damaged surfaces were extracted with high precision. The methodology proved to be a practical and economical solution for cultural heritage monitoring and conservation, offering high accuracy and flexibility. One of the greatest advantages of the method is its ease of implementation, its execution speed, and the potential of using entirely open-source software. This approach can be easily adapted to various heritage sites, significantly contributing to their protection and valorization.

Keywords: cultural heritage; photogrammetry; 3D data analysis; degradation detection; point cloud processing; algorithms; structural analysis

Citation: Caciora, T.; Ilieș, A.; Herman, G.V.; Berdenov, Z.; Safarov, B.; Bilalov, B.; Ilieș, D.C.; Baias, Ș.; Hassan, T.H. Advanced Semi-Automatic Approach for Identifying Damaged Surfaces in Cultural Heritage Sites: Integrating UAVs, Photogrammetry, and 3D Data Analysis. *Remote Sens.* **2024**, *16*, 3061. https://doi.org/10.3390/rs16163061

Academic Editors: Giulia Sammartano and Caterina Balletti

Received: 28 June 2024
Revised: 16 August 2024
Accepted: 20 August 2024
Published: 20 August 2024

1. Introduction

The preservation and analysis of cultural heritage (CH) sites are critical in maintaining their historical and architectural integrity, considering that they can be partially or fully

damaged by a series of factors, among which the ones worth mentioning are climatic, geological, and geomorphological factors, and human action [1,2]. With the advances in survey techniques, photogrammetry and 3D point cloud (PC) have become essential tools for accurately documenting and assessing the condition of these sites [3,4]. Now, the PCs and the meshes of the CH objectives obtained following the application of photogrammetric or laser scanning survey techniques can be used in many practical applications, from visualization and promotion [5–7], to evaluation and analysis [8,9], to virtual restoration [10,11].

The photogrammetric survey technique and 3D data collection through PCs (especially those that include the SfM algorithm) have become indispensable tools in documenting and assessing the conservation status of CH sites. Thus, PCs represent an efficient and accurate method for mapping and identifying damage in CH structures, offering several significant advantages [12]. They allow a quick and detailed assessment of the structural condition of the sites, eliminating the need for laborious field inspections [13]. By means of advanced laser scanning and photogrammetry techniques, large areas can be covered in a short time, which is particularly useful in managing extensive or hard-to-reach sites [14]. Modern techniques allow the capture of fine details and the exact identification of damaged surfaces (DS), including cracks and material loss, thus contributing to a better understanding of the structural condition of heritage objects [15]. The data acquisition process and subsequent analysis of the collected data are faster and less expensive compared to traditional inspection and measurement methods [16]. At the same time, PCs can be used to document and analyze sites in various environmental conditions and places inaccessible by traditional methods, making it possible to assess areas that are otherwise difficult to monitor [17].

Among the advantages that the process of PCs registers, one of the most interesting is undoubtedly their ability to identify DS within the objectives belonging to the CH. Specific techniques for detecting DS in heritage buildings using PCs acquired through imaging techniques, building information modeling (BIM), and heritage building information modeling (HBIM) include semantic segmentation based on deep learning and the use of unsupervised machine-learning methods for automatic segmentation and alteration detection. Semantic segmentation using dynamic convolutional neural networks enables the accurate recognition of architectural elements and accelerates the modeling process of historical buildings for the development of HBIM [18,19]. Brand works in the identification of different work techniques are those of Mohan and Poobal [20] and Bruno et al. [21] who proposed a compilation of an up-to-date review of them, both in terms of manual, as well as semi-automatic and automatic techniques.

Unsupervised machine-learning and clustering methods are used to automatically segment PCs and detect alterations on historical surfaces, such as chromatic variations and biological colonization, based on color information from PCs [22]. The primary objective is to automatically detect objects and data using specific algorithms to assess and monitor the condition of the objectives and to identify DS. Transfer learning and data augmentation improve the performance of semantic PC segmentation, reducing computation time and increasing model accuracy [23]. These advanced techniques contribute to the accurate and rapid assessment of structural degradations, facilitating continuous monitoring and the development of effective conservation strategies [24]. In the specialized literature, Peng and Nam [25] developed an automatic system for identifying cracks by Gaussian filter, intensity gradient, and pattern recognition; Hamrat et al. [26] implements the determination of DS based on the measurement of tensors; Muñoz-Pandiella [27] considers the use of the Gaussian filter and the random sample consensus algorithm (RANSAC) for the detection of the initial shape, while Sánchez and Quirós [28] consider that a semi-automatic detection method is optimal for the detection of degradations on a facade based on an image-based approach.

Nowadays, regarding the PC segmentation, both learning-based methods (LBMs) and non-learning-based methods (NLBMs) are used [29]. The LBM leverages machine-learning and deep-learning techniques to automatically detect and classify DS in CH objects from PC data. These methods benefit from the ability to learn from large datasets and improve their performance over time [30]. In the meantime, the NLBM typically involves traditional image processing and geometrical analysis techniques. These techniques do not rely on extensive training datasets and are often used for initial assessments or in conjunction with the LBM [22]. Even if the LBM is a more advanced technique, the NLBM has the advantage of being simple to implement and intuitive, efficient in terms of time and cost, and implemented and applied directly, and has the ability to reduce the risk of overfitting [31,32].

Therefore, affordable and adaptable methods are critically needed to evaluate the deterioration of historic buildings and CH sites. Therefore, the present study proposes the development of a technique that considers a semantic-segmentation-based approach and a semi-automated pipeline, which uses unmanned aerial vehicles (UAVs), structure from motion (SfM) and PC processing, for the detection of DS within the objectives of CH using an NLMB. The proposed method is characterized by great flexibility and can be easily replicated for most CH objectives, regardless of the geometric complexity of the investigated scenes. The segmentation algorithms and morphological and mathematical operators were applied to identify the properties of the scene and finally to classify and identify the DS. This has the advantage of being fast and economical, using open-source software and financially accessible data capturing tools, without compromising the quality of the results obtained.

Within the specialized literature, we have identified a significant gap concerning the development of low-cost methodologies for this purpose. Consequently, our approach not only involves the use of cost-effective software but also the implementation of a quick and easily deployable methodology. This methodology innovatively combines existing computational algorithms, which are integrated into a series of open-source software. By leveraging these resources, we aim to create an efficient and affordable solution for assessing the deterioration of historic structures and CH sites. At the same time, unlike other existing methods, this approach can extract DS with a high accuracy even from unstructured datasets, without the need to train a machine-learning model. The final goal of this work is to provide an efficient and accessible solution for monitoring and preserving CH, thus contributing to its protection and valorization in the current technological context.

2. Materials and Methods

To test the functionality of the developed pipeline, a 20th-century fortification located in the immediate vicinity of the Municipality of Oradea (Romania), in the Nojorid Commune, was chosen as a case study. The object is made of reinforced concrete with walls up to one meter thick (Figure 1). The specific target selected is a defense casemate, an integral part of a defensive line consisting of 320 casemates built during the Second World War, which extends over most of the western part of Romania. This line of defense has been likened by many to France's Maginot Line, which was in operation at the beginning of the Second World War. The defensive structures were partially destroyed using explosives in 1940 after the cession by Romania of this territory to Hortyste Hungary following the Vienna Dictatorship; but some can still be found in a partial state of preservation even today, while others have been reduced to a pile of rubble [33,34].

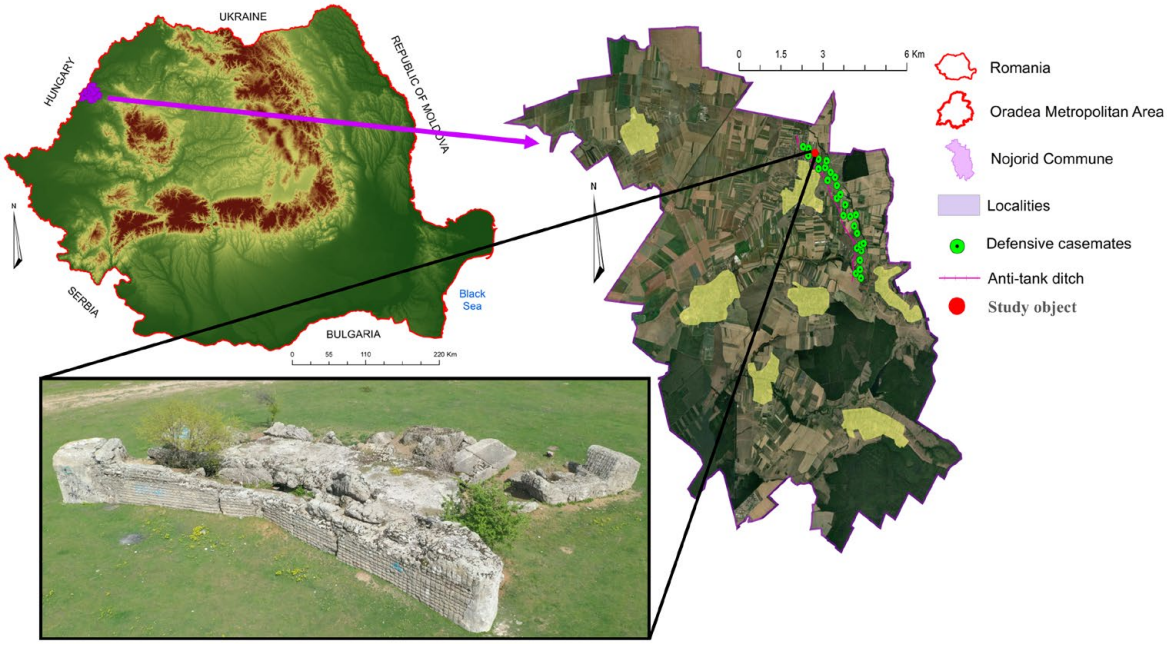

Figure 1. The location of the analyzed casemate at the level of Romania and the Nojorid commune.

This casemate, due to its state of degradation and historical relevance, provides an ideal framework for testing and validating the semi-automatic working pipeline proposed for the detection of the DS. The advanced state of degradation provides a challenging scenario for detecting the DS and extracting non-degraded surfaces (NDS), thus allowing a detailed assessment of the accuracy of the working pipeline even under severe degradation conditions. The specific historical background and complexity of the present case study are ideal to demonstrate the efficiency, accuracy, and general applicability of the developed technique.

To achieve the final results, a structured workflow was implemented, segmented into various stages. Each stage is built upon the previous one, ensuring systematic progression. Initially, the dense PC was processed to extract the points of interest. These points underwent detailed geometric analysis to identify structural features and anomalies. Subsequently, the DI algorithm quantified the extent of degradations and obtain partial results. Then, RANSAC algorithm refined the dataset by isolating inliers and eliminating outliers, at the same time, dividing the analyzed surface into types of geometric shapes. Finally, the FACETS algorithm segmented the PC into facets and families of planes, allowing the extraction of the final DS and NDS. This multi-stage workflow ensured precise and reliable structural assessment (Figure 2).

In order to test the workflow, it was decided to validate the results by including a new case study, namely, a 13th-century fortification, included in the list of historical monuments in Romania, the Cheresig Tower. It is located in the Metropolitan Area of the Municipality of Oradea, right on the western border of Romania with Hungary. It is reminiscent of a medieval fortress built in the Romanesque style, with a hexagonal plan and a height of approximately 24.7 m, arranged on 4–5 levels. The objective in question is an excellent case study for testing the methodology due to its complexity, historical context, and degree of preservation.

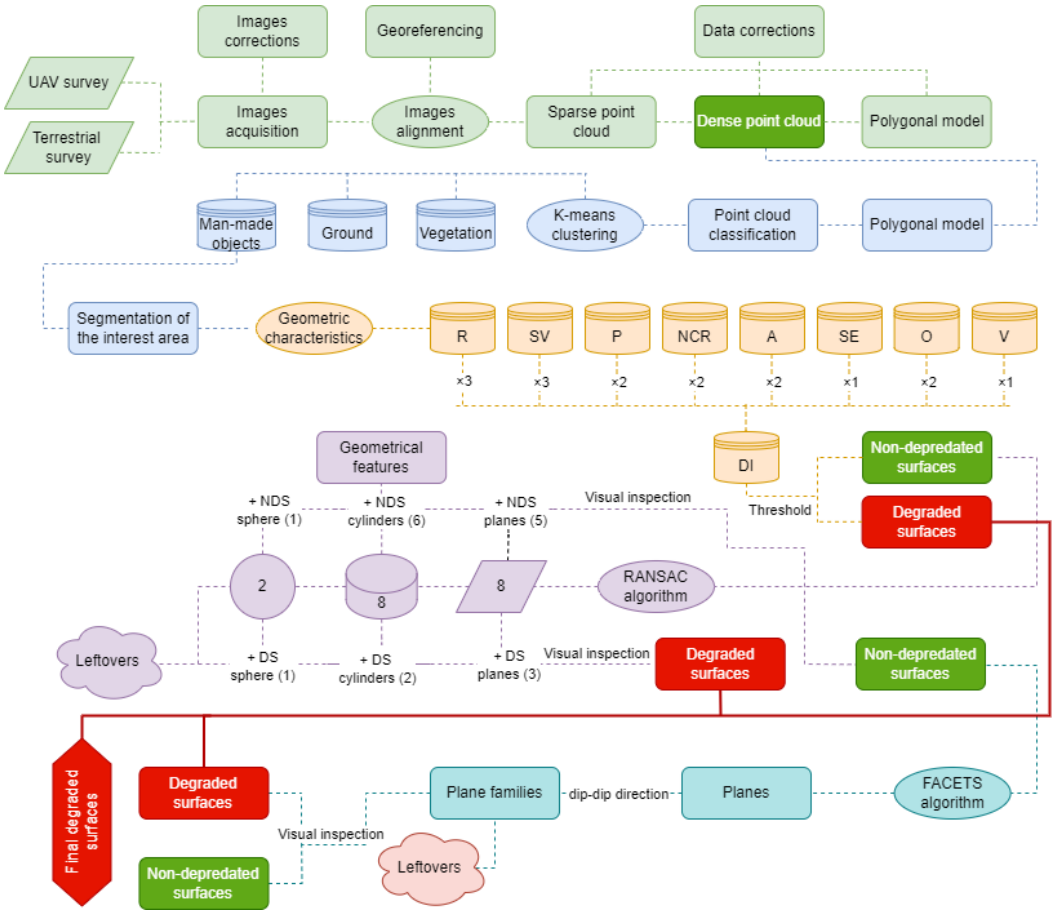

Figure 2. Implemented workflow for structural analysis and degradation detection.

2.1. Image Collection and Processing

The collection of images from the field involved capturing an area of 2185.3 using an UAV and a terrestrial photography sensor, through a process that carefully takes into account the specific techniques and practices in terms of obtaining data in the case of photogrammetry based on SfM algorithm [35,36]. The UAV used was a DJI Mavic 2 Pro equipped with a LID 20c 1" CMOS Sensor (20 MP), while the terrestrial sensor was represented by a Canon EOS R with sensor objective RF 15–35 mm F2.8 L IS US (Table 1). The UAV was controlled by means of the 3D Survey Pilot v.2.18.1 software, which allows for a careful adjustment of the flight and image acquisition parameters. Considering the complexity of the scene, the UAV photos were acquired both from nadir and with the gimbal at different angles (oblique), from the height of 10 m, 15 m, 20 m, 25 m, and 30 m; at each altitude, the flight grid was double. In the case of the photos taken with the terrestrial sensor, they were aimed at capturing in detail the features of the scene that suffered from occlusions and accentuated noise and could not be optimally acquired with the UAV. This working methodology ensured a homogeneous distribution of points within the PC, both horizontally and vertically. Moreover, in the phase of acquiring data from the field, obtaining measurements for georeferencing the model was considered, by using a Stonex S700A (Stonex SRL, Milan, Italy) with a controller Stonex S40 (Stonex SRL, Milan, Italy). These consisted of six coded ground control points (GCPs) and three check points (CPs), evenly distributed within the scene, which were measured with a GNSS GPS-RTK system to determine the real coordinates (Table 1).

Table 1. Sensors used and photogrammetry survey characteristics.

Photos Acquisition and Processing						
Camera model	DJI Mavic 2 Pro-Sensor LID 20c 1 CMOS (20 MP)					Canon EOS R-sensor objective RF 15–35 mm F2.8 L IS US
Altitudes	10 m	15 m	20 m	25 m	30 m	Ground
No. of raw photos	227	211	176	154	140	108
No. of photos after pre-processing	221	205	163	150	17	92
Camera tilt to the vertical (°)	0°–45°	0°–45°	0°	0°	0°	Between 0° and 90°
Overlapping (forward-side; %)	85–85	80–80	75–75	75–75	70–70	Between 60% and 80%; both forward and side
GSD (cm/px)	0.27	0.40	0.54	0.67	0.81	Not applicable.
Acquisition design	Double grid and circle					Circle
Image size (pix)/image bit depth (bi)	5464 × 3070/16					6720 × 4480/16
Ground control						
Sensor model	Stonex S700A with a controller Stonex S40					
Number of GCPs	6					
Number of CPs	3					
GCP dimensions (m)	1 × 1					
GCP measurement method	GNSS-RTK base and rover					
Min/Max GCP precision (XY, Z; mm)	±8/±21; ±15/±35					
Coordinate reference systems	WGS84					

The first phase in terms of image processing considered testing their quality in order to implement corrections in terms of lens and geometric distortions, and chromatic aberrations, as well as adjustments of dynamic range, sharpening, contrast, saturation, noise filtering, exposure, consistency metadata, contrast between pixels, etc. [36]. For these actions, the software Adobe Photoshop (v.25.9; Adobe Systems, San Jose, CA, USA), Agisoft Metashape (v2.1.1; Agisoft LLC, St. Petersburg, Russia) and Digital Lab Notebook Inspector (v1.0 beta; Cultural Heritage Imaging, San Francisco, CA, USA) were used. All the corrections were performed using non-destructive editing techniques to ensure that the original metadata remained intact. This was achieved by working with adjustment layers and smart objects, which allowed for changes in the features of the images without altering the original image file or its metadata. Additionally, when exporting the corrected images, care was taken to use file formats and export settings that preserved the metadata (include metadata), ensuring that all necessary information was maintained for subsequent processing in Agisoft Metashape. At the same time, there is a potential issue of image distortion related to the movement of the UAV if its speed exceeds approximately 1–1.5 m/s. In our study, the speed of the UAV was maintained below this threshold. Therefore, the rolling shutter effect was negligible, and no additional modeling was necessary for this effect [37]. It is also important to note that all sensors were stopped at the time of image capture to ensure the highest quality of the data.

The final processing of the images was implemented in Agisoft Metashape, where, before aligning all the data in a single reference space, the setting of the coordinate system was considered based on the GCPs measured in the field and the CPs. Furthermore, the generation of the four results that the software can provide (sparse PC, dense PC, mesh, and textured model) was considered. The results were cleaned, and the points considered dispensable were eliminated, each stage being optimized.

Finally, a spatial noise reduction filter was added by means of the median denoising filter technique within the PC and mesh surfaces, in order to eliminate abnormal values resulting from image processing and acquisition errors. To achieve this, quantitative and qualitative techniques were implemented to remove or correct all the points characterized

by a low base–height ratio (such as those located at the edges of the images), eliminate all less reliable points, and clean out the points characterized by significant residual values. Moreover, points with significant residual values, indicative of discrepancies between observed and modeled data, were also identified and cleaned. This step was crucial for ensuring that the final 3D model accurately represented the actual physical structure without the distortions introduced by noise and errors during the data acquisition phase. The combined application of these methods allowed for a robust noise reduction, leading to a cleaner and more precise 3D model that better represents the true geometry of the scanned surfaces. This meticulous approach ensured that the final data were of high quality, facilitating more accurate analysis and interpretation of the structural conditions.

2.2. Analysis Methods

The analysis proposed in this study is structured in four distinct stages, as follows: classification of PC; the application of the degradation index algorithm (DI), the application of the RANSAC; and the application of the FACETS algorithm. The applied algorithms were thus chosen to detect with the greatest precision the variations of the surface and the geometry of the scene, considering the fact that man-made objectives are characterized to the greatest extent as having a specific geometry and somewhat predictable shapes.

The relationship between the four stages is one of subordination and inclusiveness, each of them generating individual results and having a clearly defined objective within the methodology. But, at the same time, the obtained results work only when analyzed as a whole.

Regarding the software used to implement the algorithms, they are CloudCompare 2.13.1, MeshLab 2023.12, and Open 3D v0.18, all of these being open-source programs for advance PC processing. More precisely, CloudCompare was used for the initial stage of segmentation and classification of PCs, as well as for calculating their geometric characteristics. Furthermore, the obtained results were important in MeshLab and Open 3D to combine the features and implement DI. Finally, the RANSAC and FACETS algorithms were also implemented within CloudCompare. In order to ensure compatibility between programs and the preservation of metadata, the use of standard formats widely supported by these programs, such as ply and obj, was considered. Both formats support PCs and mesh data, including vertex, texture, and normal information.

2.2.1. Classification of the Point Clouds

For a superior knowledge of the created PCs, it is of great importance to classify them based on different characteristics. The operation includes grouping similar points within the 3D PC based on their attributes. The segmentation process is crucial for distinguishing the structural regions from components that could introduce noise into the model, particularly vegetation and other objects irrelevant for structural analysis. Among the many techniques, in the current study, a classification pipeline based on K-means-clustering-type automatic learning was chosen and implemented. K-means is a robust and efficient technique that aims to minimize the sum of the squared distances between the points in each cluster and its centroid. This allows points in a PC to be grouped into clusters based on similarities in terms of their characteristics, such as position, color, intensity, or other metric attributes [38,39].

K-means is a clustering algorithm that divides n points into k groups, where each point belongs to the group with the closest centroid. The approach considers associating each point x_i with the nearest centroid by minimizing the squared distance:

$$d^2(i,k) = \sum_{j=1}^{p} (\mathbf{x}_{ij} - \mathbf{s}_{(k)j})^2 \quad (1)$$

where $d^2(i,k)$ is the squared distance between the object i and the centroid vector k, x_{ij} is the value of the variable j for the object i, and $s_{(k)j}$ is the j value of the k centroid [40].

After the initial allocation of objects, the centroids are recalculated for each cluster according to:

$$\mathbf{x}_{(k)j} = \frac{1}{n_k}\sum_{i \in C_k} \mathbf{x}_{ij} \quad (2)$$

where $x_{(k)j}$ is the mean value of the variable j for the group k, n_k is the number of objects in the group k, and C_k represents the set of objects in the group k [40].

The two steps are iterative, repeatable until the allocations no longer change between consecutive iterations. In order to stop the iterations, we defined a threshold of 0.01 units (1 cm). This ensures that the algorithm stops once the centroids have stabilized and further iterations will not result in significant changes. This value is typically very small because the goal is to ensure that the centroids have converged to a stable position.

In the current study, PCs were classified into terrain, medium and high vegetation, and man-made objects, both by automatic and manual sampling techniques. The automatic ones were implemented through feature-based clustering (FBC), through the adaptive triangulated irregular network algorithm [41,42].

2.2.2. Application of the Degradation Index Algorithm

Based on the detailed analysis of the PCs and the information they store, various essential geometric characteristics can be extracted that have the ability to accurately indicate the DS within an objective, even if the data are unstructured. By applying advanced segmentation and classification techniques, geometric features such as planarity, roughness, and deviations from ideal shapes can be accurately quantified. The analysis of geometric features is crucial for distinguishing between DS and NDS within a structure. By measuring specific attributes, subtle variations that may indicate structural issues can be detected.

Although, in some specific contexts, certain geometric features can individually identify areas affected by degradation, in the present study the integration of several variables was considered to develop a combined index. This index shows considerable potential to be more robust and efficient in the detection and analysis of the DS, as indicated by Son et al. [43] and Capolupo [8]. The fundamental principle on which this approach is based is that DS in heritage structures are identified by detecting unusual geometric patterns [44], and a point within the PC may have low values for certain geometric features and high values for others; an approach that combines the variables has a higher accuracy and registers a more realistic composite score. This process allows the point to be more accurately classified into a specific category, thus reflecting its state of degradation and reducing classification errors.

In the realization of *DI*, we considered eight geometric variables of *PC*, respectively: roughness (*R*), surface variation (*SV*), planarity (*P*), normal change rate (*NCR*), anisotropy (*A*), sum of eigenvalues (*SE*) (derived from the covariance matrix of the local neighborhood of points in a *PC*), omnivariance (*O*), and verticality (*V*) [8,45–48]. The final algorithm is represented as:

$$\begin{aligned} DI_i = {} & w_R \cdot \sqrt{\tfrac{1}{N}\sum_{j=1}^{N}(\boldsymbol{z}_j - \overline{\boldsymbol{z}})^2} + w_{SV} \cdot \tfrac{1}{N}\sum_{j=1}^{N}\left\|\nabla_{zj} - \nabla\overline{z}\right\| + w_P \cdot \tfrac{\lambda_2-\lambda_3}{\lambda_1} + w_{NCR} \\ & \cdot \tfrac{1}{N}\sum_{j=1}^{N}\left\|\boldsymbol{n}_j - \overline{\boldsymbol{n}}\right\| + w_A \cdot \left(1 - \tfrac{\lambda_2}{\lambda_1}\right) + w_{SE} \cdot (\lambda_1 + \lambda_2 + \lambda_3) + w_O \cdot (\lambda_1 \cdot \lambda_2 \cdot \lambda_3)^{\frac{1}{3}} + w_V \\ & \cdot (1 - |\boldsymbol{n}_i \cdot \mathbf{v}|) \end{aligned} \quad (3)$$

where:

$$\mathbf{R_i} = \sqrt{\frac{1}{N}\sum_{j=1}^{N}(\mathbf{z}_j - \overline{\mathbf{z}})^2} \quad (4)$$

$$\mathbf{SV_i} = \frac{1}{N}\sum_{j=1}^{N}\left\|\nabla_{zj} - \nabla\overline{z}\right\| \quad (5)$$

$$\mathbf{P_i} = \frac{\lambda_2 - \lambda_3}{\lambda_1} \tag{6}$$

$$\mathbf{NCR_i} = \frac{1}{N}\sum_{j=1}^{N}\left\|\mathbf{n}_j - \overline{\mathbf{n}}\right\| \tag{7}$$

$$\mathbf{A_i} = 1 - \frac{\lambda_2}{\lambda_1} \tag{8}$$

$$\mathbf{SE_i} = \lambda_1 + \lambda_2 + \lambda_3 \tag{9}$$

$$\mathbf{O_i} = \lambda_1 \cdot \lambda_2 \cdot \lambda_3 \tag{10}$$

$$\mathbf{V}_i = 1 - |\mathbf{n}_i \cdot \mathbf{v}| \tag{11}$$

The equation can be simplified as:

$$\begin{aligned} DI_i = w_R \cdot \mathbf{R}_i + w_{sv} \cdot \mathbf{SV}_i + w_P \cdot \mathbf{P}_i + w_{NCR} \cdot \mathbf{NCR}_i + w_A \cdot \mathbf{A}_i + w_{SE} \cdot \mathbf{SE}_i \\ + w_O \cdot \mathbf{O}_i + w_V \cdot \mathbf{V}_i \end{aligned} \tag{12}$$

where $R_i \ldots V_i$ represent the values of the geometric variables calculated at the point i from the PC, and $w_R \ldots w_V$ represents the corresponding weight coefficient, reflecting its relative importance in determining the final degradation score (1–3).

We chose to use these geometric characteristics of the PC due to the fact that they are the most sensitive to changes in the surface and to noise [49,50], which can indicate damage. In this sense, R was chosen due to the fact that it measures the vertical variation of points in an area and is represented by the standard deviation of the altitudes of the points, SV measures the change in gradient between points, P indicates how flat a surface is, NCR measures the variation of directions of the normal vectors of the points, A measures the degree of uniformity and directionality in the distribution of points, SE indicates the total size of local variations, O reflects the diversity of local shapes, and V measures the alignment of the normal vectors to a given vertical vector [51,52].

In the present study, the DI algorithm serves as a comprehensive tool for evaluating the overall degradation state of a structure by combining various geometric features into a unified metric. This composite index provides a more nuanced and accurate representation of structural health than any single feature could.

2.2.3. Application of the RANSAC Algorithm

RANSAC is an iterative algorithm used for estimating the parameters of a mathematical model from a dataset that contains a significant proportion of outliers. It was first introduced by Fischler and Bolles in 1981 [53], and, since then, has become a standard technique in computer vision, image, and PC processing.

It is based on the idea of repeatedly selecting a random subset of the input data, fitting a model to this subset, and then evaluating how well this model fits the entire dataset. The key strength of RANSAC is its ability to cope with a high level of outliers in the input data. Unlike traditional fitting methods that may be significantly affected by outliers, this algorithm effectively ignores the outliers and focuses on the majority of the data that fits the model well [54]. For RANSAC, in order to determine the constant vector of the plane in the case of points x, y, and z, the product of the two vectors defined by these points is used [55]. The calculation of the normal vector of the plane is expressed by:

$$\mathbf{n} = (\mathbf{x}_2 - \mathbf{x}_1, \mathbf{y}_2 - \mathbf{y}_1, \mathbf{z}_2 - \mathbf{z}_1) \cdot (\mathbf{x}_3 - \mathbf{x}_1, \mathbf{y}_3 - \mathbf{y}_1, \mathbf{z}_3 - \mathbf{z}_1) \tag{13}$$

Once the vector n is calculated, it proceeds to the determination of the constant d from the plane equation $ax + by + cz + d = 0$. For this, the point $P1(x1, y1, z1)$ is used:

$$d = -(ax_1 - by_1 - cz_1) \tag{14}$$

The distance from a point $P(x,y,z)$ to the plane defined by the equation $ax + by + cz + d = 0$ is given by the formula:

$$Distance = \frac{|ax + by + cz + d|}{\sqrt{a^2 + b^2 + c^2}} \quad (15)$$

Counting the points that are at a distance smaller than a threshold (inliers) of a plane and generating the final results is carried out by:

$$Inliers = \sum_i \left(\frac{|ax_i + by_i + cz_i + d|}{\sqrt{a^2 + b^2 + c^2}} < threshold \right) \quad (16)$$

By applying the described calculation methods, RANSAC aims to determine the normal vector of a plane, its constant term, and evaluate the distance of points from this plane to identify the points that are close to it. This process is essential in determining DS within an object, contributing to a better understanding and management of the CH objects [56].

In this case, The RANSAC algorithm was applied on the PC that was considered to represent NDS that resulted from the application of the DI algorithm, in order to improve the analysis pipeline. The algorithm was chosen due to its ability to process data with a large number of outliers, its efficiency in processing large volumes of unstructured data belonging to an object with a varied geometry, and its ability to extract the essential characteristics of the structures. RANSAC leaves the possibility of a more direct and adaptable approach, reducing the need for frequent manual interventions and constant adjustments.

Therefore, the primary purpose of applying RANSAC in this case study is to improve the robustness of model fitting in the presence of noise and outliers, which are common in real-world datasets. By focusing on the majority of the data that fits a given model and ignoring the outliers, RANSAC ensures that the resulting model is representative of the actual structure.

2.2.4. Application of the FACETS Algorithm

The FACETS algorithm is used to identify and analyze planar surfaces from a 3D PC. By segmenting the surfaces into facets, the algorithm allows a detailed geometric characterization of each area of the scanned surface. Although it has multiple implementation techniques, the fast marching (FM) algorithm was chosen. FM is usually preferred for comparative analysis due to its ability to model the propagation of phenomena through a cloud of points and to detect complex structures and shapes. This is particularly relevant for degradation analysis, where modeling the propagation of damage or erosion is essential. However, it may be more complex to implement and may require more computation time for large volume data compared to KD-Tree.

FM is a numerical technique used to solve the Eikonal and static Hamilton–Jacobi equations. The Eikonal equation, essential for the FM method, is formulated as follows:

$$F(x)|\nabla T(x)| = 1 \quad (17)$$

where $T(x)$ is the arrival time at point x, and $F(x)$ is the speed function, which can vary depending on the position. In the Eikonal equation, $T(x)$ is the time required for a wave to reach point x from an initial source, and $F(x)$ is the speed of the wave at point x [57,58].

The FM technique uses finite-difference numerical schemes to compute the solutions of the Eikonal equation, being similar to Dijkstra's algorithm, but applied in the context of wavefront equations [57]. The process involves initializing a discrete grid with known arrival time values on a subset of the grid, followed by propagating them to neighboring points in increasing order of arrival time using a priority queue. At each step, the point

with the lowest current arrival time is selected and the $T(x)$ values for the neighboring points are updated according to the scheme:

$$T(i,j) = \min(T(i-1), T(i+1,j),\ T(i,j-1), T(i,j+1)) + \frac{h}{F(i,j)} \quad (18)$$

where h is the distance between grid points [57].

The FM algorithm solves the Eikonal equation using the following discretized relation:

$$\left(\frac{T_{i,j-}T_{i-1,j}}{h}\right)^2 + \left(\frac{T_{i,j-}T_{i,j-1}}{h}\right)^2 = \frac{1}{F_{i,j}^2} \quad (19)$$

This equation is solved iteratively for each grid point until all points have been processed [57].

The FACETS algorithm was applied to the NDS PC obtained from the application of the RANSAC algorithm, for a more detailed identification of the DS and the completion of the previous approach. The FACETS algorithm was chosen to improve the combined performance of the RANSAC and DI algorithms due to its ability to segregate the data into specific subsets and reduce the impact of outliers. This combination optimizes the process of identifying DS and provides a more accurate and detailed analysis.

The FACETS algorithm applied in the present workflow aims to provide a detailed geometric characterization of surfaces by segmenting large, potentially noisy areas identified by RANSAC into smaller, more accurate sub-facets. This refinement is crucial for detecting and analyzing fine degradations and subtle surface variations that may be overlooked by broader segmentation techniques.

Thus, the final degradation index (*FDI*) for identifying the DS within the PC analyzed is represented by a formula that includes multiple variables and geometric parameters to provide a comprehensive and precise assessment of the state of degradation, facilitating a robust and efficient classification of the affected areas, by:

$$FDI = \sum_{i=1}^{N} \mathbf{DI}_i + R + F \quad (20)$$

where *FDI* is the final damage index, *DI* is the degradation index calculated for each point i, R is the result of the RANSAC method applied to the set of points, and F is the result of the FACETS algorithm applied to the set of points

3. Results

3.1. Processing and Classification of the Point Clouds

The initial dense PC, generated based on the detailed results of the photogrammetric survey, contained a total of 5,643,759 individual coordinates (Figure 3a). This significant amount of spatial data allowed a faithful and precise reconstruction of the analyzed surfaces, providing a solid basis for further evaluations of geometric features and the identification of the DS. The analyses to determine the reprojection error (RE) indicated a combined average value of 0.087 m, while the root mean square error (RMSE) values are built up by a value of 0.071 m for the X coordinate, 0.074 for the Y coordinate, and 0.069 for Z coordinate. The obtained RE and RMSE values are indicative of a high-precision measurement system and a faithful model.

The PC classification analyses based on FBC and by K-means indicated that the most extensive category is the one that presents points related to the ground (48.75%), closely followed by mad-made objects (46.51%) and medium and high vegetation (4.74%) (Figure 3b).

In the segmentation process, PC was classified to isolate points corresponding to man-made objects. From this subset, the southeastern wall of the objective was selected for detailed analysis. Despite significant deterioration, this section of the wall was chosen due to its high fidelity in representing the authentic characteristics of the casemate (Figure 3). The PC data for the wall comprised 1,123,085 individual coordinates. To facilitate an easier

implementation of the analyses, considering hardware and software resources, and given the sufficient density and quality of the PC, the data were decimated by approximately 61%, resulting in a refined PC containing 433,856 points. This processed dataset was then used to identify and analyze the DS.

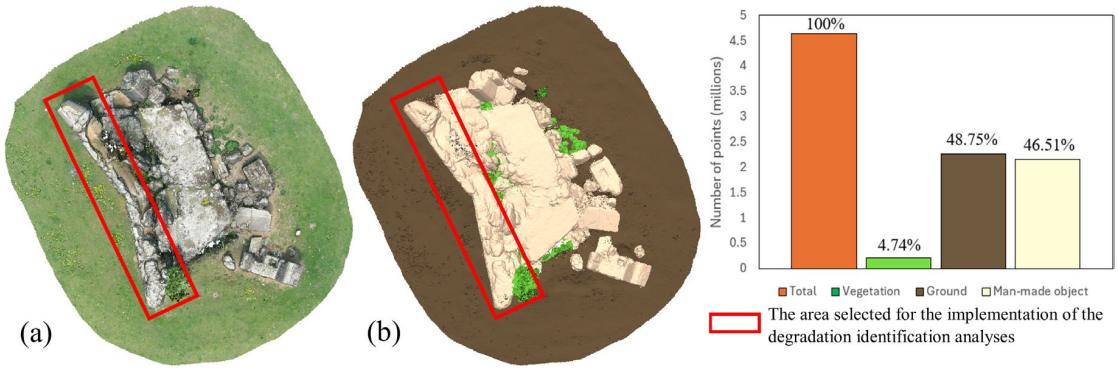

Figure 3. The dense PC of the analyzed casemate and the classification of points according to class, in vegetation, ground, and man-made object ((**a**) the dense PC of raw points; and (**b**) the dense PC of classified points).

3.2. Implementation of the Analyses for the Determination of Damaged Surfaces

3.2.1. Implementation of the Degradation Index Algorithm

All analyses regarding the determination of the geometric characteristics of the scene were performed using a sphere with a radius set to 0.1 m. This was implemented considering the fact that it is small enough to capture fine details of the wall surface. This is important for detecting microcracks, roughness, and other irregularities that could indicate degradation. This radius was chosen to balance between capturing enough detail and avoiding overloading unnecessary data. A larger radius could lose fine details, while a smaller radius could introduce excessive noise into the data, as stated by Demantké et al. [59].

The determination of the eight indicators was carried out by establishing the geometric characteristics, calculating the normal gradient and curvature through the norms plug-in and eigenvalues using PCA. The results were exported in a scalar field with most of the values between 0 and 1 (1 as the maximum value), where the value 0 represents a coordinate that has the lowest possible value for that feature compared to all other points in the PC (smooth surface and the absence of gradient variations, in the present case), while a value closer to 1 indicates uneven, rough, and unorganized surfaces. The results obtained after the extraction of the geometric characteristics of the scene were at the basis for the application of the formula developed for extracting the DI (Figure 4). It was implemented within the datasets by defining the arithmetic formula that includes the normalized scalar fields and the associated weights for each characteristic. The implementation of the weights involves multiplying each normalized scalar field by the appropriate weight. The weights assigned to each indicator reflect their relative importance within the model and for detecting differences regarding the surface of PCs. Features that may directly indicate severe structural defects, such as R and SV, are given higher weights, while features of more general or indirect relevance, such as SE and V, are given minimal weights (Figure 4). R and SV received the highest weighting (3) because they directly measure surface irregularities and changes, which are strong indicators of degradation. P and NCR were given a weight of 2 because they are essential for evaluating the flatness and changes in the direction of the normal vectors of the surfaces; and A and O (and those with weight 2) provide information about the uniformity and diversity of local forms. SE and V received the lowest weighting (1) due to their more general or indirect relevance in damage detection. In this case study, the decision to assign these weights was based on the sensitivity of each feature to surface changes and noise, ensuring that the model accurately reflects the degradation state of the analyzed PCs.

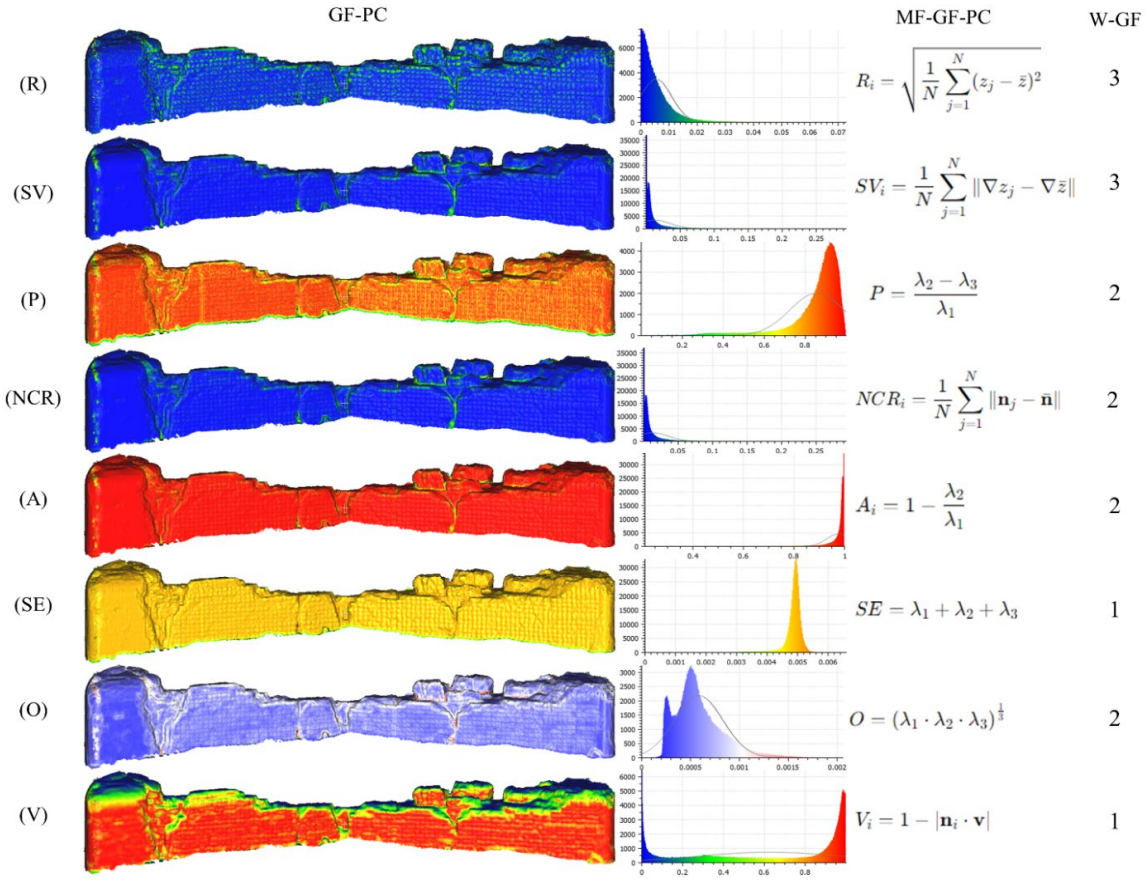

Figure 4. The results obtained for the eight geometric characteristics of the analyzed PC (GF-PC—geometric features of the PC; MF-GF-PC—the mathematical formula for calculating the geometric characteristics of the PC; and W-GF—the weight of the geometric features in the final model).

The formula's application resulted in the obtaining of a new dataset that indicates the DS of the analyzed PC with greater precision. The generation of the histogram of the scalar field values for the composite index provides a broad perspective on the distribution of the values and helps the operator to identify the thresholds for determining the DS (Figure 5a). Hence, it was identified that all the values that are above the threshold of 68.62% (0.065) in terms of fidelity to the model represent DS. The threshold was manually identified by means of detailed visual examinations of the DS and by systematically comparing them with the obtained results. These points, amounting to 136,813 individual coordinates, were segmented from the rest of the PC and exported in an individual scalar field. After applying the formula for combining geometric features into a composite index, we noticed that the vast majority of degradations are represented by deep cracks and areas where the material is completely missing. These findings are clearly illustrated in Figure 5b.

Although the DI algorithm accurately identified surface changes of PC indicating the DS, it also has limitations. These consist of the fact that some areas of the model are erroneously identified as NDS. This occurs where surfaces do not show significant variations in the analyzed features, such as a large surface variation, drastic changes in normal vectors, or major structural variations. Flat surfaces or those with subtle variations in geometric features are not effectively detected by the current model, even though, upon closer analysis, they may show obvious signs of degradation (Figure 6).

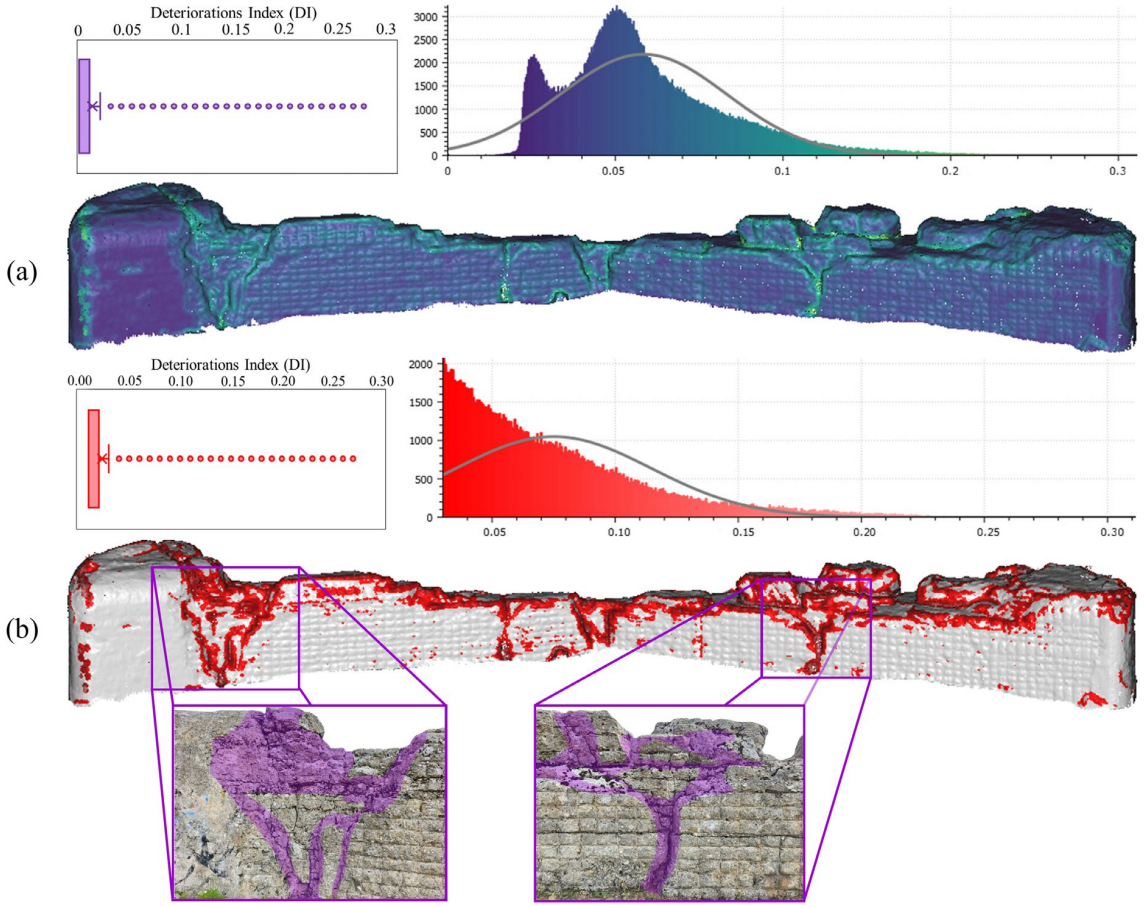

Figure 5. (**a**) Visual representation and statistical distribution of DI values for the original dataset, and (**b**) visual representation and statistical distribution of DI values for the independent dataset within the model and on the real object.

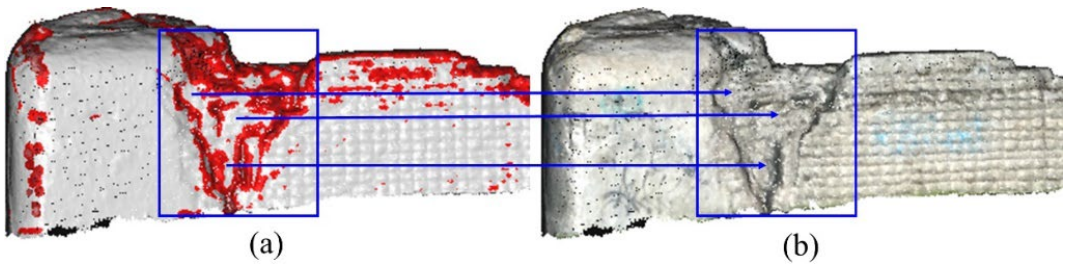

Figure 6. The identification of the limitations of the created DI algorithm, due to the recognition of some flat surfaces without surface changes as NDS, even if they are part of a more extensive DS ((**a**) the results obtained for DI within the analyzed PC; and (**b**) the PC visualization in RGB).

3.2.2. Implementation of the RANSAC Algorithm

To address the limitations identified in the initial DI model, it was decided to insert the RANSAC algorithm into the geometric feature analysis. RANSAC contributes to improving the model quality by reducing false positive and false negative errors, ensuring that fine degradations are properly detected and non-damaged planar surfaces are not misclassified.

The RANSAC algorithm was configured with a distance threshold of 0.01 units and a maximum number of 10,000 iterations to exhaustively explore the solution space. A minimum percentage of 90% of the points had to match the model for validation, and the probability of success was set at 99%. These strict settings allowed the accurate isolation of planar surfaces and other relevant structures, reducing false positive errors.

The algorithm segmented PC into eight individual planes, eight cylindrical shapes, and two spheres (Figure 7 and Table 2). But, in the present case, the most important characteristics of the scene that RANSAC can determine are the leftovers points. Considering that RANSAC works by multiple random iteration of a subset of points in the PC and adjusting a geometric model, if they are inside the optimal distance threshold, the points are considered to be inliers (and, therefore, included in the model), and those that do not match are outliers (leftovers) [60]. In the present case, leftovers represent with great accuracy the presence of surface changes, degradations, or structural peculiarities within PCs. The leftovers category was represented by 26,726 individual points (Figure 7f). The model refinement analysis indicated that all leftovers are attributed to DS, or to areas that are not of interest for the segmentation of the NDS.

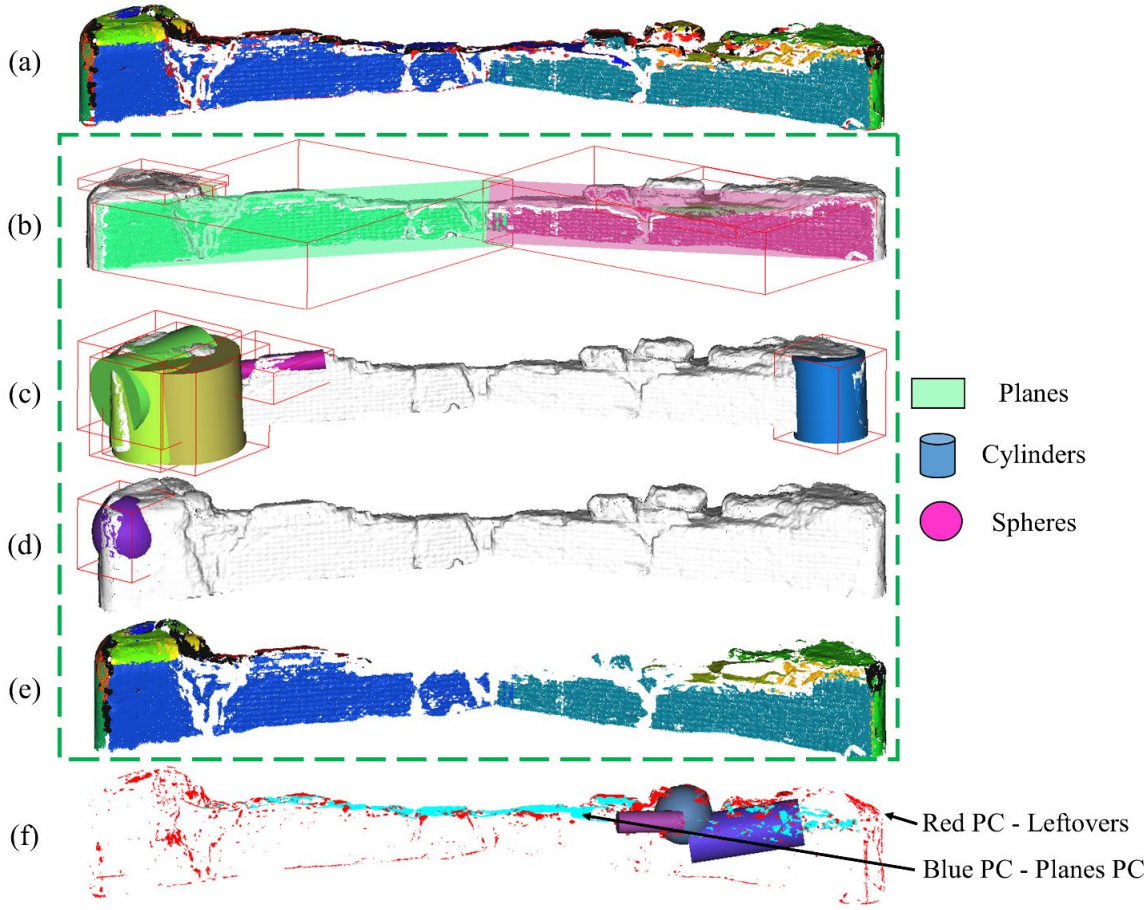

Figure 7. The results generated following the implementation of the RANSAC algorithm on the datasets related to the NDS obtained after the DI analysis ((**a**) the initial dataset after the application of RANSAC; (**b**) the planes considered to be part of NDS; (**c**) the cylindrical geometric shapes considered to be part of NDS; (**d**) the spherical geometric shapes considered to be part of NDS; (**e**) the independent datasets considered to be part of NDS, after the elimination of non-conforming values; and (**f**) the independent datasets considered to be part of DS, represented by PC and geometric shapes).

Table 2. The individual values for the three geometric shapes obtained after applying RANSAC on the analyzed datasets.

Plane	Dip	Dip-Dir	DR	Cylinder	r	h	DS	Sphere	r	DS
P1	88°	217°	NDS	C1	1.29	2.94	NDS	S1	0.82	DS
P2	87°	243°	NDS	C2	1.1	2.51	NDS	S2	0.97	NDS
P3	43°	45°	DS	C3	1.19	3.3	NDS			
P4	10°	52°	DS	C4	1.4	2.73	NDS			
P5	5°	25°	NDS	C5	1.68	2.91	NDS			
P6	4°	155°	NDS	C6	0.29	3.52	NDS			
P7	77°	95°	NDS	C7	0.66	3.22	DS			
P8	41°	258°	DS	C8	0.3	1.84	DS			

NDS—non-degraded surfaces; DR—data relevance; r—radius (sphere, cylinder); DS—damaged surfaces ; Dip-Dir—dip direction; h—height (cylinder).

In addition to the points categorized by the algorithm as leftovers, within the geometric shapes obtained by RANSAC, some that present DS were also identified. To extract them, basic principles were applied regarding the plans generated by the algorithm and the general knowledge about the objectives of this kind. Consequently, dip-dip values (inclination and direction of inclination) were used to differentiate planes that show DS from those that do not. Undamaged planes were determined to have dip-dip values indicating a stable and uniform orientation. In general, they tend to be planes closer to vertical or horizontal, suggesting surfaces that remained intact and were not subjected to forces that would significantly deform them. These planes may represent structural sections of the wall that are better preserved, having a better structural integrity due to their orientation, which did not allow the accumulation of excessive stress. For example, they could be (depending on the scene) as close as possible to 0° or 90°, with an azimuth dip of any value between 0° and 360°. In the case of the casemate, the planes considered optimal had dip-dip values of 88°–217°, 87°–243°, 5°–25, 4°–155°, and 77°–95° (five such planes) (Figure 5b and Table 2).

Planes considered to represent DS have dip-dip values that indicate an uneven and often unusual orientation. They are tilted in a way that suggests they have been subjected to external forces such as erosion, cracking, or structural movements that caused deviations from their original position. They can vary in a wide spectrum and can record many different dip-dip values. After validation with the help of the initial data captured in the PC for the analyzed casemate, the elimination of three planes was considered due to the non-uniformities with the general structure, characteristics that indicate damage. These had dip-dip directions of 43°–45°, 10°–52°, and 41°–258° (Table 2). A pattern becomes evident when we compare the dip-dip values of the planes considered intact with the degraded ones, but all the values were previously validated, for high accuracy.

Not only were planes exhibiting damage based on dip-dip values eliminated, but certain cylindrical and spherical models were also excluded (Figure 7c,d). The exclusion of these patterns was not solely based on specific threshold values; rather, it was validated against the original datasets. The analyzed object features partially curved surfaces, with cylindrical and spherical shapes being significant. Therefore, the validation process ensured that these geometric forms were accurately represented, eliminating those that were incorrectly identified as degraded based on their geometric characteristics alone. However, two cylinders and a sphere were considered based on empirical validation to represent false positive surfaces, rather attributed to DS zones. They have a pattern and a well-defined geometric structure representative of NDS surfaces, but they are actually detached pieces from the basic objective, which acts independently. These are not of interest for the analysis to determine NDS in the present case, being therefore categorized as DS (Figure 7f and Table 2).

3.2.3. Implementation of the FACETS Algorithm

Although RANSAC improves the results of the analysis, there are still some areas categorized as false positives and, therefore, included as NDS. These are especially related to points assigned based on geometric features as belonging to the same shape (predominantly planes), even when there are significant surface differences between them and the rest of the coordinates in that plane. This leads to an inaccurate representation of the structure and introduces noise into the final model (Figure 8a). The errors may occur due to algorithm limitations in handling local surface variations and inherent noise in the collected data. Areas of small but significant degradation are often incorrectly attributed to dominant geometric forms such as planes. These degradations are critical to the ultimate success of the model as they influence the structural integrity of the walls. A correct identification and removal of the points that represent DS are crucial in order to ensure model accuracy and prevent structural interpretation errors.

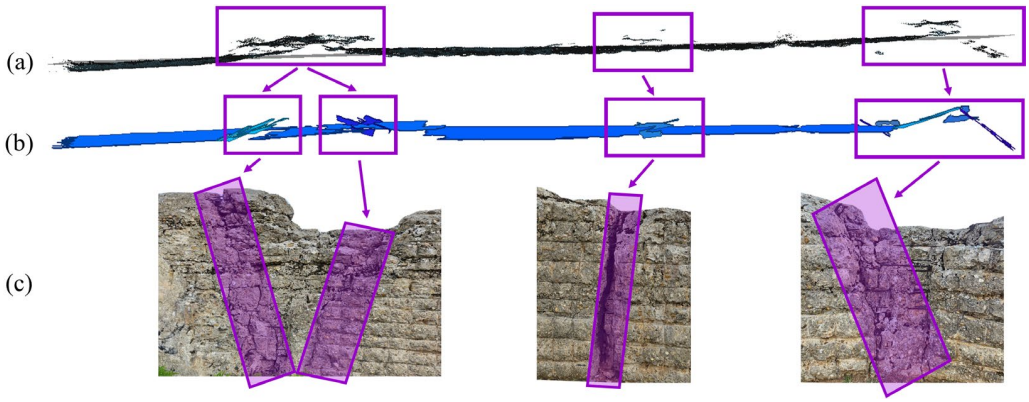

Figure 8. The identification of some limitations of the geometric representations generated by the RANSAC algorithm, due to the recognition of slightly different surfaces from the normal as belonging to the same plane and how they can be determined with greater accuracy by the FACETS algorithm ((**a**) PC belonging to the same plane-which therefore, it must be represented by surfaces with similar characteristics; (**b**) dividing the same PC by facets into different families of planes; and (**c**) visualization of areas with shortcomings within the real object).

The solution for eliminating the shortcomings left after the implementation of the RANSAC algorithm is to refine the methodology by integrating other filtering and post-processing algorithms, such as the FACETS algorithm. It allows the subdivision and refinement of surfaces detected by RANSAC, more precisely, identifying transition zones and subtle surface differences. It locally analyzes the structure of the PC, generating facets that better match the fine variations of the surface. In the case of a large plane identified by RANSAC that includes significant variations, FACETS can segment this surface into smaller and more precise sub-facets, more faithfully reflecting the real structure (Figure 8b).

For the FACETS algorithm, the object size was set to small values, between 0.5 and 2 units, allowing a detailed analysis and the detection of fine degradations. The RMS distance threshold was set to values between 0.01 and 0.05 units, ensuring that only points that closely matched the generated facet were included, thereby eliminating noise and outliers. The algorithm was configured to run a maximum number of 10,000 iterations to fully explore the adjustment possibilities and find the best matches for the facets. A minimum percentage of 90% of the points was required to accept a geometric model, thus ensuring that only models with a significant fit were accepted. Noisy point filtering has been enabled, applying a strict threshold to remove them and thus reducing the impact of noise on the quality of the generated facets. The type of surface selected was predominantly planar, reflecting the prevailing structure of the walls, with adjustments for curvilinear forms where the specific geometry dictated.

In the case of FACETS, the same PC segmentation principle was implemented as in the case of the RANSAC results. Thus, NDS planes were considered those with dip-dip values indicating stable orientations, such as near-vertical or near-horizontal angles. Plans that indicate decay usually have more varied and less stable values, suggesting potential structural problems. Values can be spread over a wider range without being clustered near stable orientations. The analysis of the frequencies of dip directions and dip angles between non-degrading and degrading plane families shows significant differences.

For most families that represent NDS, it was taken into account that the most common dip directions are 15° and 75° while dip directions such as 165°, 225°, and 255° occur less frequently. In contrast, dip families show a greater variety of dip directions, including angles such as 105°, 195°, 315°, and 345°. The frequencies of dip angles indicate that, in NDS families, angles of 15° and 75° are the most common, while, in families with degradation, the angle of 45° is more common. It is thus observed that families of planes with DS tend to have a more diverse set of dip directions and angles, especially angles of 45°, compared to those with NDS, which are more concentrated around specific angles such as 15° and 75° (Figure 9 and Table 3). In this way, 14 families of planes that are assigned to NDS were individualized and segmented, respectively, and 16 families of planes that represent DS. Within them, only two families come out of the stability pattern above, these being F12 in the case of NDS, and F21 in the case of DS, which, although they have dip-dip values, can fit to some extent within the other category compared to the one in which they were distributed. In the case of F12, it is the only family within NDS that records dip directions of 45°, and F21 is the family with the lowest value of dip angles (highlighted in red in Table 3). Although unusual, they were assigned to the respective categories after a careful validation of the FACETS results with the initial database, in order to refine and eliminate outliers (Figure 9).

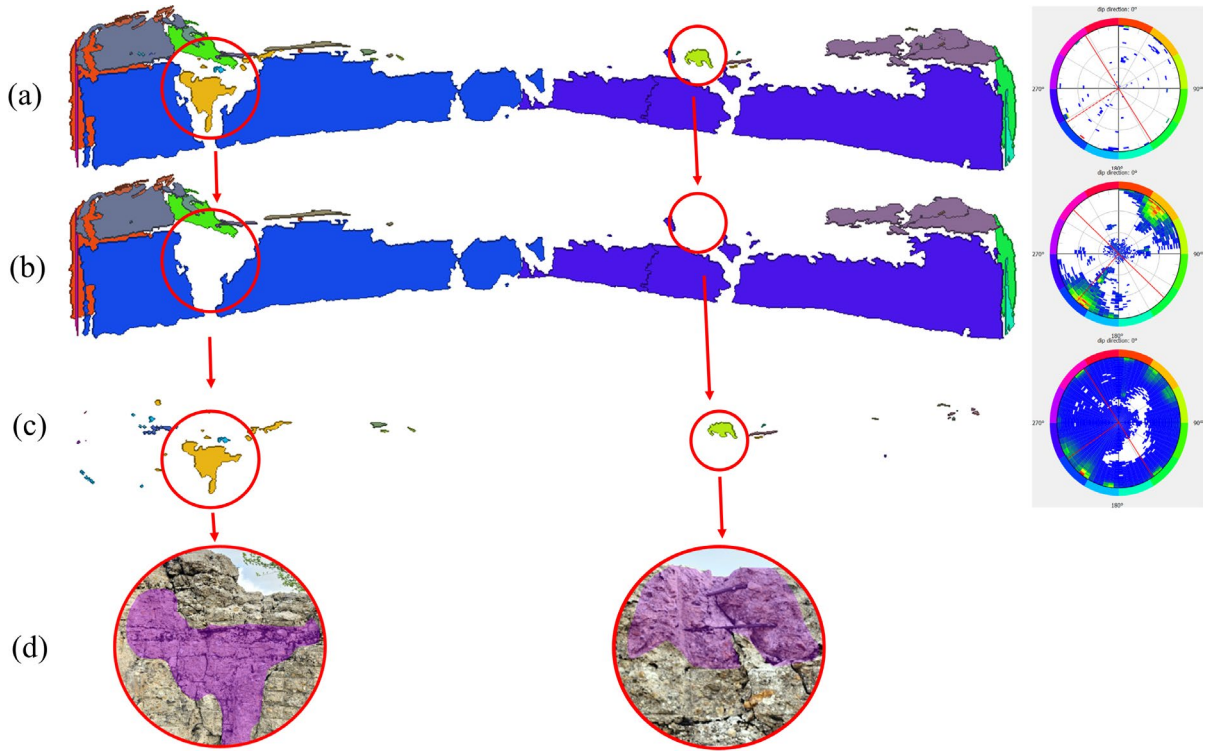

Figure 9. The results obtained after the implementation of the FACETS algorithm on the datasets related to the NDS obtained after the RANSAC analysis ((**a**) the initial dataset after the application of FACETS, represented according to the family; (**b**) the independent datasets considered to be NDS; (**c**) the sets of independent data considered to be DS; and (**d**) visualization of areas with shortcomings within the real object).

Table 3. The values obtained for each family of plans following the implementation of the FACETS algorithm.

NDS	Dip-Dip Dir.	No. F	RMS	DS	Dip-Dip Dir.	No. F	RMS
F1	15°–15°	2	0.04; 0.001	F3	55°–15°	4	0.002; 0.006; 0.002; 0.001
F2	45°–15°	3	0.002; 0.007; 0.002	F4	105°–15°	1	0.003
F5	165°–15°	1	0.04	F6	195°–15°	1	0.001
F7	225°–15°	4	0.001; 0.08; 0.008; 0.005	F10	315°–15°	1	0.002
F8	255°–15°	2	0.008; 0.002	F11	345°–15°	4	0.005; 0.002; 0.003; 0.001
F9	285°–15°	4	1.79; 1.60; 0.05; 0.02	F13	75°–45°	2	0.003; 0.004
F12	15°–45°	9	0.001; 0.001; 0.08; 0.001; 0.001; 0.001; 4.20; 0.001; 0.001	F14	165°–45°	1	0.004
F20	15°–75°	5	0.001; 0.07; 0.001; 0.001	F15	195°–45°	2	0.002; 0.001
F23	105°–75°	1	0.07	F16	225°–45°	8	0.004; 0.002; 0.001; 0.001; 0.001; 0.001; 0.002; 0.005
F24	135°–75°	1	0.09	F17	255°–45°	1	0.002
F25	165°–75°	2	0.02; 0.001	F18	285°–45°	1	0.001
F27	225°–75°	4	0.05; 0.02; 0.007; 0.002	F19	345°–45°	1	0.002
F28	255°–75°	8	0.003; 0.009; 0.002; 0.01; 0.05; 0.05; 0.002; 0.005	F21	45°–75°	10	0.003; 0.005; 0.004; 0.01; 0.002; 0.004; 0.01; 0.004; 0.001; 0.002
F30	315°–75°	1	0.03	F22	75°–75°	2	0.002; 0.009
				F26	195°–75°	10	0.001; 0.001; 5.1; 0.001; 0.001; 0.001; 0.001; 0.002; 0.003; 0.003
				F29	285°–75°	1	6.2

Dip-Dip Dir.—dip-dip directions; NDS—non-degraded surfaces; no. F—number of facets per family; DS—damaged surfaces; RMS—root mean square—indicates the degree of match between the adjusted facet and the original points in the PC.

3.2.4. Final Results Obtained for Degraded Surfaces and Non-Degraded Surfaces

The results indicate that the PC of the DS is represented by 202,502 individual coordinates, and that of the NDS is individualized by 230,892 points. Most of the points that registered DS were segmented after the implementation of the DI algorithm (31.5%), 13.8% being individualized after the RANSAC algorithm, and, after the application of FACETS, 1.4% of the points were eliminated, the remaining 0.1% of the points being eliminated from the model due to the fact that they were redundant. The PCs obtained after the implementation of the DS were further processed to extract the polygonal surfaces, for quantitative and qualitative analyses on the mesh. They indicated that, out of the object's total surface of 109.9 m^2, the DS represents 48.3 m^2 (43.5%), and the remaining 61.6 m^2 (56.5%) of the surfaces are classified as NDS (Figure 10).

3.2.5. Validation of the Results

In order to validate the results obtained in the previous stage, the use of the same indicators regarding the geometric characteristics and the calculation algorithms used was considered. Unlike the case study represented by the casemate, within the Cheresig Tower, the only changes were in the weights that were given to the geometric characteristics in the model and in the thresholds set for RANSAC and FACETS. Otherwise, the workflow followed remained identical, and the user's intervention to adjust it was minimal (Figure 11). These changes were performed due to the volume of points that make up the PC (3,658,453 individual coordinates), the characteristics of the monument, and the visual inspections that took place in situ and within the eight components of the DI.

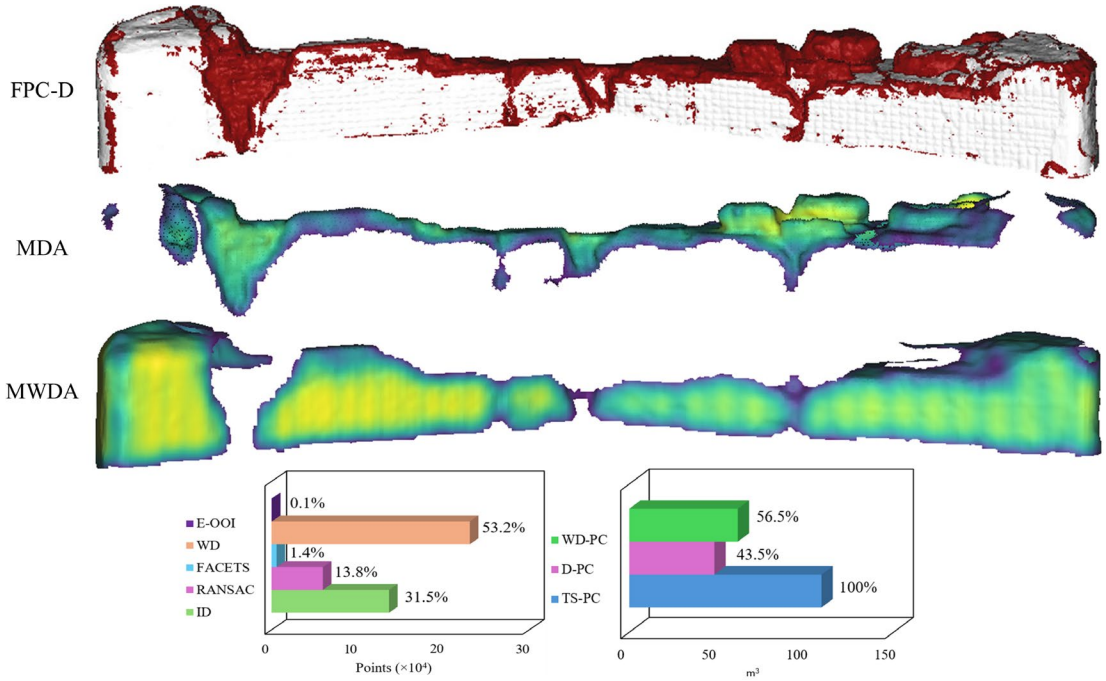

Figure 10. The spatial distribution of the areas that recorded DS and NDS within the PC of the analyzed casemate and their quantitative and qualitative analysis (FPC-DS—final PC that represents DS; MDA—major damage areas; MWDA—major areas without damages; DI—the degradations identified following the DI algorithm implementation; RANSAC—degradations identified by RANSAC algorithm; FACETS—degradations identified by FACETS algorithm; E-OOI—points removed because they were outside the area of interest; and TS-PC—total surface of the model).

The geometric features were determined in a sphere with a radius of 0.1 m, so that even the finest details of the tower could be captured, but large enough to optimize the computational time and avoid introducing noise into the data. In this context, the highest weights were assigned to the SV, NCR, and V (3), followed by R, P, and O (2), while A and SE were considered to have a relatively low importance within the model (1). The application of the DI algorithm led to the segmentation of a PC in 563,767 points (representing 15.4% of the total area of the fortification), which was considered to represent DS, following the application of a threshold of 48.31% (all values below this threshold were classified as DS, while values above it were assigned to NDS) (Figure 12). After combining the DS into a composite index, it was found that most of the degradations are represented by the lack of material and deep cracks, and most of them are inside the monument (Figure 11).

The application of the RANSAC algorithm on the PC identified as part of the DS following the DI analysis was configured with a distance threshold of 0.1 units between primitives, a resolution of 0.2 units, and a maximum deviation from the normal of 25°. The algorithm was run with a maximum number of 10,000 iterations to explore the solution space, requiring a minimum of 90% of the points to match the proposed model, a 99% probability of success, and a minimum of 1000 support points per primitive. Following this configuration, 28 planes, 20 cylinders, 5 spheres, and 174,717 leftovers were generated (Figure 12). Of the generated geometric shapes, four planes and three cylinders were assigned to the DS class (16,693 points), being considered as false positive surfaces; planes showed dip-dip directions that did not align with scene features to a standard close to 0° or 90°, while the assignment of cylinders to the DS class was made based on visual inspections. Finally, a total of 191,410 points were removed from the model because they represented DS (Figure 11).

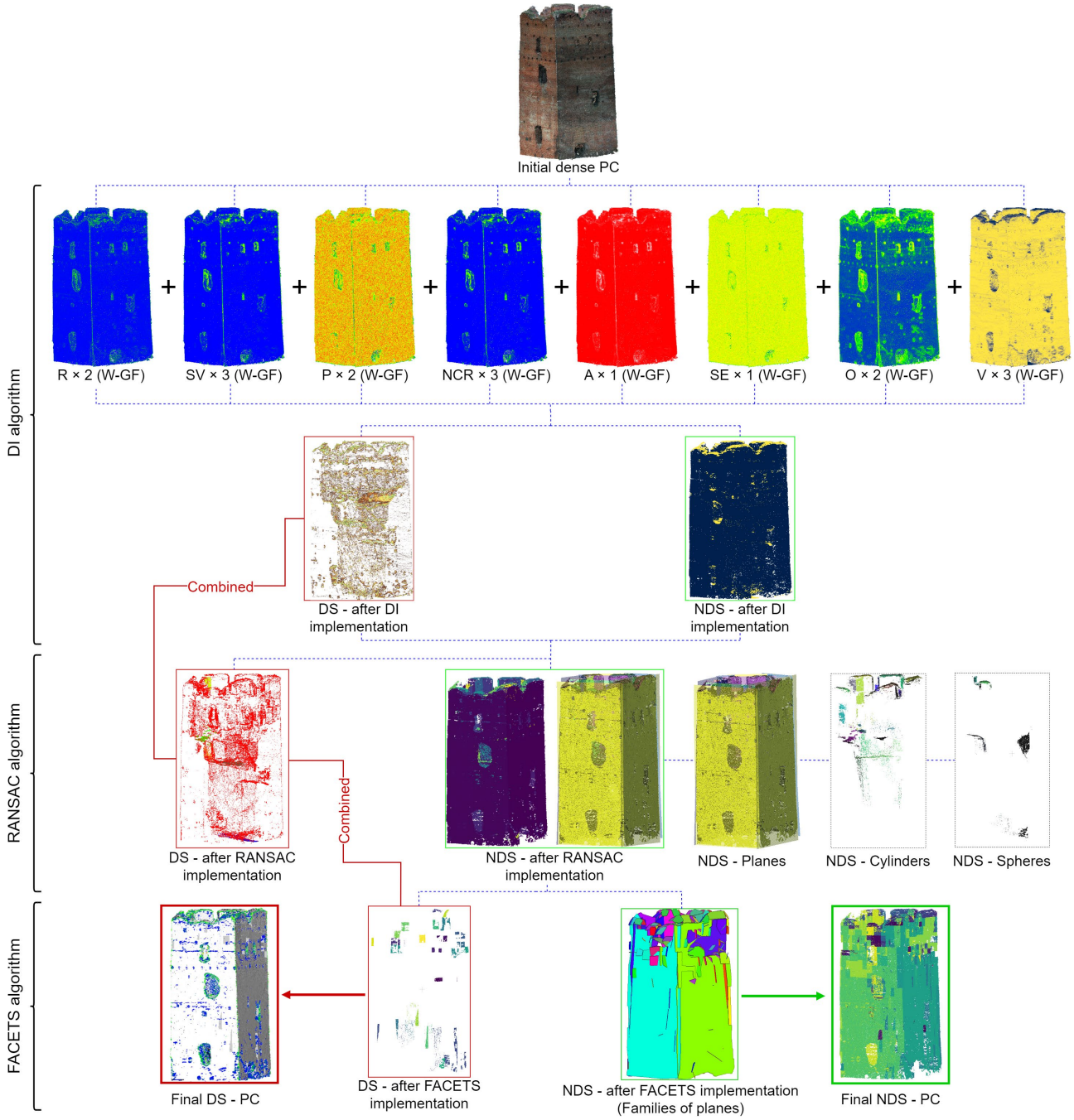

Figure 11. Implementation of the DI, RANSAC, and FACETS within the Cheresig Tower and obtaining the final DS and NDS.

The PCs containing NDS, obtained from the application of the RANSAC algorithm, were exported to a separate entity and subjected to FACETS-based analyses. The parameters set for this analysis included a relative distance of 2 units with a maximum angle of 20° and a maximum distance of 99%, an RMS distance threshold of 0.01 units, and a maximum number of 10,000 iterations. The implementation of the FACETS algorithm resulted in the generation of 186 facets, which were compressed into 34 plane families. Of these, 29 were considered to represent NDS, and five were assigned to DS (Figure 11). Plane families that did not align with the pattern, according to visual inspection, showed dip-dip directions of 195°–75°, 225°–75°, 15°–15°, 45°–15°, and 15°–45°, having dip angles of 15°, 45°, or 75° as

a common point. Finally, the families of plans considered to be DS after applying FACETS were represented by a total of 31,335 points (Figure 12).

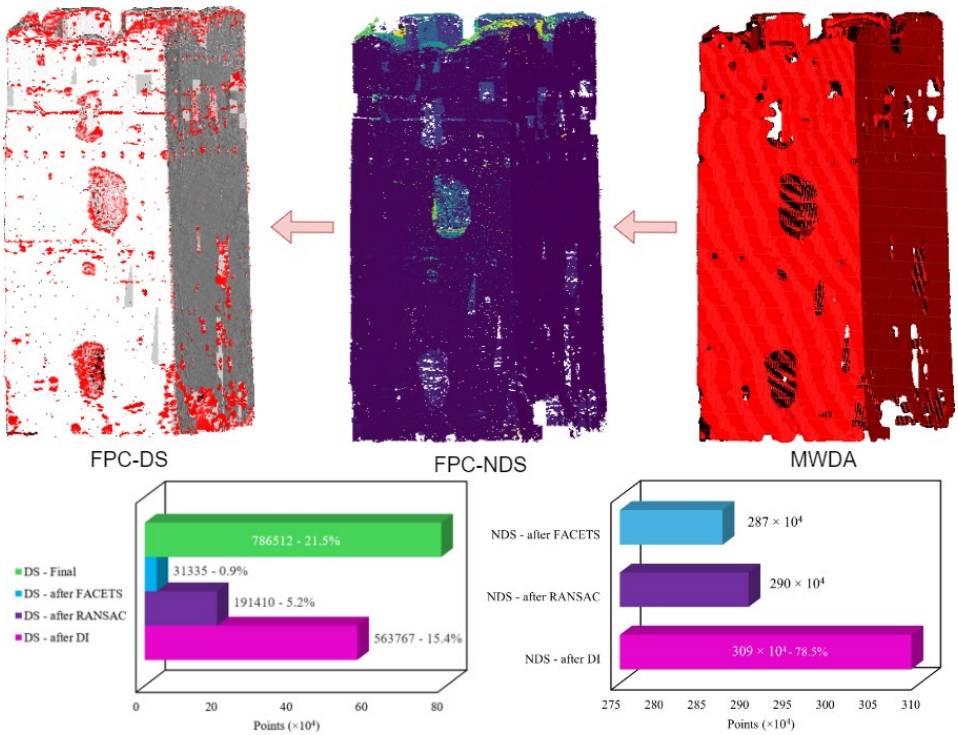

Figure 12. The spatial distribution of the areas that recorded DS and NDS within the PC of the analyzed historical structure and their quantitative and qualitative analysis (the graphs show the number of points related to DS eliminated after each stage, respectively, and the number of points associated with NDS obtained after each stage).

Finally, the results obtained after applying the workflow on the analyzed fortification show that DS are represented by 786,512 points, and NDS are individualized by 2,871,941 individual coordinates. In the case of DS, most points were segmented after the application of DI (15.4%), followed by RANSAC (5.2%) and FACETS (0.9%), the total area allocated to this group being 21.5%. The processing of the two obtained PCs (DS and NDS) in order to extract the polygonal surfaces and their analysis indicated that, of the total surface of 1447.84 m^2 of the model, the DS represents 311.29 m^2, and the remaining 1136.55 m^2 of the surfaces are classified as NDS (Figure 12).

4. Discussion

The results demonstrate that the approach is considerably accurate in identifying the DS. The method is robust in identifying very fine degradations and minor surface differences, which is crucial for the detailed monitoring and prevention of major structural problems. As indicated by Zang et al. [61], the use of the geometric characteristics of the PC for the identification of DS is very efficient. However, there are notable limitations of the model. This is also observable in our interpretation, where, although DI has identified most of the DS, a high sensitivity can lead to the overestimation of degradation in certain areas, or, on the contrary, a low sensitivity can generate false negative areas. Studies in the field [62–64] indicate that these shortcomings are determined both by data noise and especially by variations in the local geometry of the scene.

The use of RANSAC improved the detection process of fine degradations and small surface differences, identifying cracks and areas where material is missing within the NDS PC identified by DI. It was used by several authors [65,66] to improve the feature extraction pipeline and eliminate mismatched points. In the present case, RANSAC complemented

the DI algorithm by its ability to detect essential characteristics, thus contributing to a more detailed representation of the structural state of the walls. By effectively filtering noise, RANSAC enabled a more accurate analysis and improved the overall model quality by conforming to visually observed DI [67]. Although the RANSAC algorithm is robust and efficient in detecting the predominant geometric shapes in the PCs, it also presents certain limitations and introduces noise into the final model.

The implementation of FACETS on the obtained PCs (after RANSAC) thus improves the results obtained by segregating the data into subsets based on specific characteristics, reducing the impact of outliers and improving the accuracy of the estimated model, evaluating the performance of the combined index in different subsets to optimize accuracy, identifying complex interactions between variables and providing clear data visualizations for interpreting patterns and trends [68]. Thus, the combined use of the three algorithms contributes to a deeper understanding of the behavior of DS within such a typology of monuments.

Such a combination of algorithms leaves the possibility of applying the developed methodology to wider typologies of CH monuments, as indicated by Donato and Giuffrida [69]. The combination of DI, with RANSAC and FACETS, can highlight the monuments' DS without the methodological pipeline being modified, or with minor modifications. The same situation is found in the present study, where, between the two case studies, only certain features were slightly changed (geometric feature weights and thresholds), while the rest of the workflow remained unchanged. At the same time, the vast majority of applications in the field [70] have in mind the extraction of DS only from PCs that indicate flat areas, but the model developed in this work has the ability to extract characteristics from a wide variety of PCs, provided that the analyzed object registers a more or less obvious geometric shape (plane, cylinder, sphere, curvilinear, etc.). At the same time, DS are most often analyzed based on level breaks, since they are generally located at a greater depth than the remaining surface [71,72]. But some situations are individualized in which changing the threshold value does not accurately identify DS, because, in some areas, even if they have a different depth and record an individual slope, they can still represent NDS. The elimination of these shortcomings was implemented through a combined RANSAC-FACETS algorithm, but also through the manual validation of the results, which makes the method semi-automatic.

Even if some studies consider a completely automatic approach for feature extraction [73], this is very difficult to implement and registers errors, due to the complexity of the CH elements and the various types of degradation. This is also indicated by Galantucci and Fatiguso [74], who mention that it is almost impossible to identify unique threshold values, which give significant results in all the cases in which they are applied. Specific attention must be paid to the areas where vegetation arranged on the object was identified before the segmentation of the PCs, areas that record even more noise, a factor that requires a thorough filtering process to eliminate the possible inconveniences determined by this fact [8]. Thus, most applications must also consider a post-production intervention performed by the user, in order to evaluate the accuracy of the results and, possibly, to make changes in the critical parameters. Even if all the steps are followed with the greatest fidelity, the results are determined to some extent by the skills of the operator in terms of the acquisition, manipulation, and processing of the data [75,76]. The methodology delineated in this manuscript has undergone extensive validation, confirming its general efficacy and robustness across various contexts. This process is divided into two distinct phases, the method-tuning phase and the validation phase, each utilizing different datasets to ensure the reliability and robustness of the proposed approach. The initial phase focuses on method tuning, particularly the choice of thresholds. The thresholds are carefully selected to balance sensitivity and specificity, ensuring the accurate identification of degraded surfaces while minimizing false positives and negatives. The validation step is crucial in order to verify that the chosen thresholds and algorithm settings have the potential to extract DS in a compressive way. This phase independently assesses the accuracy and reliability of the method by comparing the algorithm's outputs with manually recognized degradation features, the process being repeated for each stage of the workflow. Simultaneously, this

stage also involved the inclusion of a new case study, aiming to test the applicability of the methodology within different typologies of CH and a more extensive data volume.

Nevertheless, its application to distinct case studies may necessitate slight modifications in the threshold parameters utilized and might involve the inclusion of a more comprehensive array of geometric variables, or different thresholds for each algorithm depending on the desired quality. This underscores the necessity for fine-tuning the method to address the unique attributes and specificities inherent to each individual case study, with particular emphasis on the careful selection and adjustment of specific thresholds. Despite these variations, the core principle underpinning the methodology remains invariant. Consequently, it is imperative that the results produced at each stage of implementation undergo rigorous validation by the user to ensure the accuracy, reliability, and overall validity of the findings.

Although one of the main features of the methodology is its potential to be easy to implement and very fast, execution times are relative and depend on numerous factors such as available material resources, user experience, database size, etc. However, this approach can be optimized to be faster and more reliable, given that the main stages are fully automated, and only the inspection and minor corrective interventions are performed manually. Using algorithms that support each other in minimizing individual limitations helps improve accuracy. In addition, open-source software and accessible data capture tools are used, making the whole methodology more economical and affordable.

5. Conclusions

The methodology presented in this manuscript demonstrates the efficiency and applicability of a semi-automatic method for detecting DS within CH sites, using a structured workflow and advanced photogrammetry and PC processing techniques. The choice of the casemate as a case study allowed testing the methodology in a real and complex context, providing relevant results for heritage conservation. Moreover, the validation of the results on an architectural monument (fortification) from the 13th century highlights the extended applicability of the method in the identification of DS in the field of CH. The developed technique proved to be fast, economical, and flexible, allowing for the accurate assessment of DS even from unstructured datasets. The implementation of classification and segmentation algorithms such as K-means clustering, RANSAC, and FACETS, together with a combined index encompassing multiple geometric features of the scene, contributed to obtaining detailed results and improving the accuracy of assessments. Analysis has shown that the DS can be accurately identified, including cracks and areas where material is missing, thus contributing to a better understanding of the structural condition of heritage objects. The proposed method demonstrated a robust and efficient ability to detect fine degradations and subtle surface differences, facilitating continuous monitoring and appropriate conservation interventions. The use of PC and photogrammetry techniques allows the capture of fine details and the exact identification of DS, thus contributing to a better understanding of the structural condition of CH objects. Although the method identified most of the DS, a high sensitivity may lead to the overestimation of degradation in certain areas, and a low sensitivity may generate false negative and positive areas. The RANSAC algorithm has improved the process of detecting fine degradations and small surface differences, but it also has some limitations that introduce noise into the final model. The combined algorithm methodology has the potential to be applied to a wide range of heritage monument typologies with minor modifications to the methodological pipeline. The manual validation of the results and the adjustment of critical parameters are essential to ensure model accuracy.

In conclusion, this semi-automated NLMB provides a practical and affordable solution for CH monitoring and conservation, with the potential for wide applicability and continuous improvement through the integration of new techniques and analysis algorithms. The developed method proved to be a valuable tool for the structural health monitoring of CH sites, thus contributing to their protection and valorization in the current technological context. Besides the fact that it offers good results, the method also has the advantage of being very fast and cheap, being able to be implemented exclusively by using open-source software and

cheap sensors for data capture and processing. For future work, we are considering extending the work methodology to other types of heritage objects, improving the work methodology by implementing efficient noise reduction and outlier detection algorithms, and implementing longitudinal analyses to identify the progression of degradation over time.

Author Contributions: T.C.—conceptualization, methodology, writing—original draft, formal analysis, and supervision; A.I.—data curation, investigation, writing—original draft, and validation; G.V.H.—supervision, formal analysis, and resources; Z.B.—software, and visualization; B.S.—writing—original draft, and data curation; B.B.—writing—review and editing, and methodology; D.C.I.—visualization, validation, and investigation; Ș.B.—data curation, and writing—review and editing; T.H.H.—investigation, and data curation. All authors have read and agreed to the published version of the manuscript.

Funding: This work was supported by the Deanship of Scientific Research, Vice Presidency for Graduate Studies and Scientific Research, King Faisal University, Saudi Arabia [Grant No. KFU241319].

Data Availability Statement: The raw data supporting the conclusions of this article will be made available by the authors, without undue reservation.

Acknowledgments: The research undertaken was made possible by the equal scientific involvement of all the authors concerned.

Conflicts of Interest: The authors declare no conflicts of interest.

Abbreviations

PC	point cloud
DI	degradation index algorithm
RANSAC	random sample consensus algorithm
R	roughness
SV	surface variation
P	planarity
NCR	normal change rate
A	anisotropy
SE	sum of eigenvalues
O	omnivariance
V	verticality
FBC	feature-based clustering
NDS	non-degraded surfaces
DS	damaged surfaces
FM	fast marching
RE	reprojection errors
RMSE	root mean square error
RMS	root mean square
BIM	building information modeling
HBIM	heritage building information modeling
UAV	unmanned aerial vehicle
SfM	structure from motion
GCPs	ground control points
CPs	check points
LMB	learning-based methods
NLMB	non-learning-based methods

References

1. Ilies, D.C.; Caciora, T.; Herman, G.V.; Ilieș, A.; Ropa, M.; Baias, Ș. Geohazards affecting cultural heritage monuments. A complex case study from Romania. *GeoJ. Tour. Geosites* **2020**, *31*, 1103–1112. [CrossRef]
2. Le, T.D.; Le, T.A.; Nguyen, P.H.; Ho, Y.T.P.; Le, B.H.P. Factors affecting the decision of selecting a destination for international tourists at the Hoi an world cultural heritage site. *GeoJ. Tour. Geosites* **2023**, *51* (Suppl. S4), 1663–1675. [CrossRef]
3. Caciora, T.; Herman, G.V.; Ilieș, A.; Baias, Ș.; Ilieș, D.C.; Josan, I.; Hodor, N. The Use of Virtual Reality to Promote Sustainable Tourism: A Case Study of Wooden Churches Historical Monuments from Romania. *Remote Sens.* **2021**, *13*, 1758. [CrossRef]

4. Caciora, T.; Jubran, A.; Ilies, D.C.; Hodor, N.; Blaga, L.; Ilies, A.; Grama, V.; Sebesan, B.; Safarov, B.; Ilies, G.; et al. Digitization of the Built Cultural Heritage: An Integrated Methodology for Preservation and Accessibilization of an Art Nouveau Museum. *Remote Sens.* **2023**, *15*, 5763. [CrossRef]
5. Franczuk, J.; Boguszewska, K.; Parrinello, S.; Dell'Amico, A.; Galasso, F.; Gleń, P. Direct use of point clouds in real-time interaction with the cultural heritage in pandemic and post-pandemic tourism on the case of Kłodzko Fortress. *Digit. Appl. Archaeol. Cult. Herit.* **2022**, *24*, e00217. [CrossRef]
6. Poux, F.; Valembois, Q.; Mattes, C.; Kobbelt, L.; Billen, R. Initial User-Centered Design of a Virtual Reality Heritage System: Applications for Digital Tourism. *Remote Sens.* **2020**, *12*, 2583. [CrossRef]
7. Craiut, L.; Bungau, C.; Bungau, T.; Grava, C.; Otrisal, P.; Radu, A.-F. Technology Transfer, Sustainability, and Development, Worldwide and in Romania. *Sustainability* **2022**, *14*, 15728. [CrossRef]
8. Capolupo, A. Accuracy Assessment of Cultural Heritage Models Extracting 3D Point Cloud Geometric Features with RPAS SfM-MVS and TLS Techniques. *Drones* **2021**, *5*, 145. [CrossRef]
9. Galanakis, D.; Maravelakis, E.; Pocobelli, D.P.; Vidakis, N.; Petousis, M.; Konstantaras, A.; Tsakoumaki, M. SVD-based point cloud 3D stone by stone segmentation for cultural heritage structural analysis—The case of the Apollo Temple at Delphi. *J. Cult. Herit.* **2023**, *61*, 177–187. [CrossRef]
10. Moyano, J.; Nieto-Julián, J.E.; Lenin, L.M.; Bruno, S. Operability of Point Cloud Data in an Architectural Heritage Information Model. *Int. J. Archit. Herit. Conserv. Anal. Restor.* **2022**, *16*, 1588–1607. [CrossRef]
11. Grifoni, E.; Vannini, E.; Lunghi, I.; Faraioli, P.; Ginanni, M.; Santacesarea, A.; Fontana, R. 3D multi-modal point clouds data fusion for metrological analysis and restoration assessment of a panel painting. *J. Cult. Herit.* **2024**, *66*, 356–366. [CrossRef]
12. Herban, S.; Costantino, D.; Alfio, V.S.; Pepe, M. Use of Low-Cost Spherical Cameras for the Digitisation of Cultural Heritage Structures into 3D Point Clouds. *J. Imaging* **2022**, *8*, 13. [CrossRef] [PubMed]
13. Barazzetti, L.; Binda, L.; Scaioni, M.; Taranto, P. Photogrammetric survey of complex geometries with low-cost software: Application to the 'G1' temple in Myson, Vietnam. *J. Cult. Herit.* **2011**, *12*, 253–262. [CrossRef]
14. Grussenmeyer, P.; Alby, E.; Landes, T.; Koehl, M.; Guillemin, S.; Hullo, J.; Assali, P.; Smigiel, E. Recording approach of heritage sites based on merging point clouds from high resolution photogrammetry and terrestrial laser scanning. *ISPRS-Int. Arch. Photogramm. Remote Sens. Spat. Inf. Sci.* **2012**, *XXXIX-B5*, 553–558. [CrossRef]
15. Yastikli, N. Documentation of cultural heritage using digital photogrammetry and laser scanning. *J. Cult. Herit.* **2007**, *8*, 423–427. [CrossRef]
16. Mostafavi, A.; Scaioni, M.; Yordanov, V. Photogrammetric solutions for 3D modeling of cultural heritage sites in remote areas. In Proceedings of the ISPRS WG IV/3, WG I/8 & WG II/4ISPRS International GeoSpatial Conference 2019, Joint Conferences of 5th Sensors and Models in Photogrammetry and Remote Sensing (SMPR) and 3rd Geospatial Information Research (GI Research) (Volume XLII-4/W18), Karaj, Iran, 12–14 October 2019; Volume XLII-4-W18, pp. 765–772. [CrossRef]
17. Fryskowska, A.; Stachelek, J. A no-reference method of geometric content quality analysis of 3D models generated from laser scanning point clouds for hBIM. *J. Cult. Herit.* **2018**, *34*, 95–108. [CrossRef]
18. Adhikari, R.S.; Moselhi, O.; Bagchi, A. Image-based retrieval of concrete crack properties for bridge inspection. *Autom. Constr.* **2014**, *39*, 180–194. [CrossRef]
19. Jaradat, M.; Al Majali, H.; Bendea, C.; Bungau, C.C.; Bungau, T. Enhancing Energy Efficiency in Buildings through PCM Integration: A Study across Different Climatic Regions. *Buildings* **2023**, *14*, 40. [CrossRef]
20. Mohan, A.; Poobal, S. Crack detection using image processing: A critical review and analysis. *Alex. Eng. J.* **2018**, *57*, 787–798. [CrossRef]
21. Bruno, S.; De Fino, M.; Fatiguso, F. Historic Building Information Modelling: Performance assessment for diagnosis-aided information modelling and management. *Autom. Constr.* **2018**, *86*, 256–276. [CrossRef]
22. Musicco, A.; Galantucci, R.; Bruno, S.; Verdoscia, C.; Fatiguso, F. Automatic point cloud segmentation for the detection of alterations on historical buildings through an unsupervised and clustering-based machine learning approach. *ISPRS Ann. Photogramm. Remote Sens. Spat. Inf. Sci.* **2021**, *2*, 129–136. [CrossRef]
23. Matrone, F.; Martini, M. Transfer learning and performance enhancement techniques for deep semantic segmentation of built heritage point clouds. *Virtual Archaeol. Rev.* **2021**, *12*, 73–84. [CrossRef]
24. Rodrigues, F.; Cotella, V.; Rodrigues, H.; Rocha, E.; Freitas, F.; Matos, R. Application of Deep Learning Approach for the Classification of Buildings' Degradation State in a BIM Methodology. *Appl. Sci.* **2022**, *12*, 7403. [CrossRef]
25. Peng, S.; Nam, H. A Robust Crack Filter Based on Local Gray Level Variation and Multiscale Analysis for Automatic Crack Detection in X-ray Images. *J. Electr. Eng. Technol.* **2016**, *11*, 1035–1041. [CrossRef]
26. Hamrat, M.; Boulekbache, B.; Chemrouk, M.; Amziane, S. Flexural cracking behavior of normal strength, high strength and high strength fiber concrete beams, using Digital Image Correlation technique. *Constr. Build. Mater.* **2016**, *106*, 678–692. [CrossRef]
27. Muñoz-Pandiella, I.; Akoglu, K.; Bosch, C.; Rushmeier, H. Towards semi-automatic scaling detection on flat stones. *Eurograph. Assoc.* **2017**, *2017*, 49–58. [CrossRef]
28. Sánchez, J.; Quirós, E. Semi-automatic detection and classification of materials in historic buildings with low-cost photogrammetric equipment. *J. Cult. Herit.* **2017**, *25*, 21–30. [CrossRef]
29. Kong, X.; Hucks, R.G. Preserving our heritage: A photogrammetry-based digital twin framework for monitoring deteriorations of historic structures. *Autom. Constr.* **2023**, *152*, 104928. [CrossRef]

30. Pierdicca, R.; Paolanti, M.; Matrone, F.; Martini, M.; Morbidoni, C.; Malinverni, E.; Frontoni, E.; Lingua, A. Point Cloud Semantic Segmentation Using a Deep Learning Framework for Cultural Heritage. *Remote Sens.* **2020**, *12*, 1005. [CrossRef]
31. Moropoulou, A.; Labropoulos, K.; Delegou, E.; Karoglou, M.; Bakolas, A. Non-destructive techniques as a tool for the protection of built cultural heritage. *Constr. Build. Mater.* **2013**, *48*, 1222–1239. [CrossRef]
32. Boonpook, W.; Tan, Y.; Xu, B. Deep learning-based multi-feature semantic segmentation in building extraction from images of UAV photogrammetry. *Int. J. Remote Sens.* **2021**, *42*, 1–19. [CrossRef]
33. Mosincat, C.; Tarau, A. *Evacuarea Judeţelor din Nord-Vestul Transilvaniei (1940) şi Consecinţele Acesteia Asupra Judeţului Bihor [The Evacuation of the Counties from the North-West of Transylvania (1940) and Its Consequences on Bihor County]*; Editura TIPO MC: Oradea, Romania, 2005.
34. Mosincat, C. *Cazemata [The Casemate]*; Editura TIPO MC: Oradea, Romania, 2021.
35. James, M.R.; Antoniazza, G.; Robson, S.; Lane, S.N. Mitigating systematic error in topographic models for geomorphic change detection: Accuracy, precision and considerations beyond off-nadir imagery. *Earth Surf. Process. Landf.* **2020**, *45*, 2251–2271.
36. Martínez-Fernández, A.; Serrano, E.; Pisabarro, A.; Sánchez-Fernández, M.; de Sanjosé, J.J.; Gómez-Lende, M.; Rangel-de Lázaro, G.; Benito-Calvo, A. The Influence of Image Properties on High-Detail SfM Photogrammetric Surveys of Complex Geometric Landforms: The Application of a Consumer-Grade UAV Camera in a Rock Glacier Survey. *Remote Sens.* **2022**, *14*, 3528. [CrossRef]
37. Zhou, Y.; Daakir, M.; Rupnik, E.; Pierrot-Deseilligny, M. A two-step approach for the correction of rolling shutter distortion in UAV photogrammetry. *ISPRS J. Photogramm. Remote Sens.* **2020**, *160*, 51–66. [CrossRef]
38. Kong, D.; Xu, L.; Li, X.; Li, S. K-Plane-Based Classification of Airborne LiDAR Data for Accurate Building Roof Measurement. *IEEE Trans. Instrum. Meas.* **2014**, *63*, 1200–1214. [CrossRef]
39. Simoniello, T.; Coluzzi, R.; Guariglia, A.; Imbrenda, V.; Lanfredi, M.; Samela, C. Automatic Filtering and Classification of Low-Density Airborne Laser Scanner Clouds in Shrubland Environments. *Remote Sens.* **2022**, *14*, 5127. [CrossRef]
40. Steinley, D. K-means clustering: A half-century synthesis. *Br. J. Math. Stat. Psychol.* **2006**, *59*, 1–34. [CrossRef]
41. Becker, C.; Rosinskaya, E.; Häni, N.; D'Angelo, E.; Strecha, C. Classification of Aerial Photogrammetric 3D Point Clouds. *Photogramm. Eng. Remote Sens.* **2018**, *84*, 287–295.
42. Anders, N.; Valente, J.; Masselink, R.; Keesstra, S. Comparing Filtering Techniques for Removing Vegetation from UAV-Based Photogrammetric Point Clouds. *Drones* **2019**, *3*, 61. [CrossRef]
43. Son, S.W.; Kim, D.W.; Sung, W.G.; Yu, J.J. Integrating UAV and TLS Approaches for Environmental Management: A Case Study of a Waste Stockpile Area. *Remote Sens.* **2020**, *12*, 1615. [CrossRef]
44. Pathak, R.; Saini, A.; Wadhwa, A.; Sharma, H.; Sangwan, D. An object detection approach for detecting damages in heritage sites using 3-D point clouds and 2-D visual data. *J. Cult. Herit.* **2021**, *48*, 74–82. [CrossRef]
45. Friedman, A.; Pizarro, O.; Williams, S.B.; Johnson-Roberson, M. Multi-Scale Measures of Rugosity, Slope and Aspect from Benthic Stereo Image Reconstructions. *PLoS ONE* **2012**, *7*, e50440. [CrossRef]
46. Demantké, J.; Vallet, B.; Paparoditis, N. Streamed Vertical Rectangle Detection in Terrestrial Laser Scans for Facade Database Production. *ISPRS Ann. Photohrammetry Remote Sens. Spat. Inf. Sci.* **2012**, *I-3*, 99–104. [CrossRef]
47. Hackel, T.; Wegner, J.D.; Schindler, K. Fast Semantic Segmentation of 3D Point Clouds with Strongly Varying Density. *ISPRS Ann. Photogramm. Remote Sens. Spat. Inf. Sci.* **2016**, *III-3*, 177–184. [CrossRef]
48. Bui, A.; Apley, D. An exploratory analysis approach for understanding variation in stochastic textured surfaces. *Comput. Stat. Data Anal.* **2019**, *137*, 33–50. [CrossRef]
49. Hubert, M.; Rousseeuw, P.J.; Vanden Branden, K. ROBPCA: A New Approach to Robust Principal Component Analysis. *Technometrics* **2005**, *47*, 64–79. [CrossRef]
50. Nurunnabi, A.; Belton, D.; West, G. Robust statistical approaches for local planar surface fitting in 3D laser scanning data. *ISPRS J. Photogramm. Remote Sens.* **2014**, *96*, 106–122. [CrossRef]
51. Zhang, Y.; Guo, Q.; Wang, Z.; Yang, D. Quantitative evaluation for small surface damage based on iterative difference and triangulation of 3D point cloud. *Meas. Sci. Technol.* **2018**, *29*, 035601. [CrossRef]
52. Mohammadi, M.; Wood, R.; Wittich, C. Non-Temporal Point Cloud Analysis for Surface Damage in Civil Structures. *ISPRS Int. J. Geo-Inf.* **2019**, *8*, 527. [CrossRef]
53. Fischler, M.A.; Bolles, R.C. Random Sample Consensus: A Paradigm for Model Fitting with Applications to Image Analysis and Automated Cartography. *Commun. ACM* **1981**, *24*, 381–395. [CrossRef]
54. Raguram, R.; Frahm, J.-M.; Pollefeys, M. A Comparative Analysis of RANSAC Techniques Leading to Adaptive Real-Time Random Sample Consensus. *Lect. Notes Comput. Sci.* **2008**, *5303*, 500–513.
55. Mitropoulou, A.; Georgopoulos, A. An Automated Process to Detect Edges in Unorganized Point Clouds. *ISPRS Ann. Photogramm. Remote Sens. Spat. Inf. Sci.* **2019**, *IV-2/W6*, 99–106.
56. Li, P.; Wang, M.; Fu, J.; Wang, Y. Plane Detection Based on an Improved RANSAC Algorithm. In Proceedings of the 2023 IEEE 3rd International Conference on Computer Communication and Artificial Intelligence (CCAI), Taiyuan, China, 26–28 May 2023; pp. 211–215. [CrossRef]
57. Sethian, J.A. Fast Marching Methods. *SIAM Rev.* **1999**, *41*, 199–235.
58. Yatziv, L.; Bartesaghi, A.; Sapiro, G. O(N) implementation of the fast marching algorithm. *J. Comput. Phys.* **2006**, *212*, 393–399.
59. Demantké, J.; Mallet, C.; David, N.; Vallet, B. Dimensionality Based Scale Selection in 3D Lidar Point Clouds. *ISPRS-Int. Arch. Photogramm. Remote Sens. Spat. Inf. Sci.* **2011**, *3812*, 97–102.

60. Sun, L. DANIEL: A Fast and Robust Consensus Maximization Method for Point Cloud Registration with High Outlier Ratios. *Inf. Sci.* **2021**, *614*, 563–579.
61. Zang, Y.; Li, B.; Xiao, X.; Zhu, J.; Meng, F. An Efficient Probabilistic Registration Based on Shape Descriptor for Heritage Field Inspection. *ISPRS Int. J. Geo-Inf.* **2020**, *9*, 759. [CrossRef]
62. Mohammadi, M.E.; Wood, R.L. Identification of Key Geometrical Features for Automatic Structural Damage Detection from Point Clouds. *Struct. Health Monit.* **2017**, *2017*, 566–572. [CrossRef]
63. Huang, A.; Xie, Q.; Wang, Z.; Lu, D.; Wei, M.; Wang, J. MODNet: Multi-offset point cloud denoising network customized for multi-scale patches. *Comput. Graph. Forum* **2022**, *41*, 109–119. [CrossRef]
64. Bai, Y.; Durand, J.; Forbes, F.; Vincent, G. Semantic segmentation of sparse irregular point clouds for leaf/wood discrimination. *arXiv* **2023**, arXiv:2305.16963. [CrossRef]
65. Sun, Q.; Zhang, Y.; Wang, J.; Gao, W. An improved FAST feature extraction based on RANSAC method of vision/SINS integrated navigation system in GNSS-denied environments. *Adv. Space Res.* **2017**, *60*, 2660–2671. [CrossRef]
66. Canaz Sevgen, S.; Karsli, F. An improved RANSAC algorithm for extracting roof planes from airborne lidar data. *Photogramm. Rec.* **2020**, *35*, 40–57. [CrossRef]
67. Tang, F.; Wang, J.; Wang, Z.; Xiao, M. Research on Ransac Filtering Optimization Method of Steel Structure Buildings Based on Morphological Features. In Proceedings of the IGARSS 2022—2022 IEEE International Geoscience and Remote Sensing Symposium, Kuala Lumpur, Malaysia, 17–22 July 2022; pp. 7673–7676. [CrossRef]
68. Li, J.; Hu, Q.; Ai, M. GESAC: Robust graph enhanced sample consensus for point cloud registration. *ISPRS J. Photogramm. Remote Sens.* **2020**, *167*, 363–374.
69. Donato, E.; Giuffrida, D. Combined Methodologies for the Survey and Documentation of Historical Buildings: The Castle of Scalea (CS, Italy). *Heritage* **2019**, *2*, 2384–2397. [CrossRef]
70. Zvietcovich, F.; Castañeda, B.; Perucchio, R. 3D solid model updating of complex ancient monumental structures based on local geometrical meshes. *Digit. Appl. Archaeol. Cult. Herit.* **2015**, *2*, 12–27.
71. Kaur, N.; Tiwari, P.S.; Pande, H.; Agrawal, S. Utilizing Advance Texture Features for Rapid Damage Detection of Built Heritage Using High-Resolution Space Borne Data: A Case Study of UNESCO Heritage Site at Bagan, Myanmar. *J. Indian Soc. Remote Sens.* **2020**, *48*, 1627–1638.
72. Sarmadi, H.; Yuen, K. Early damage detection by an innovative unsupervised learning method based on kernel null space and peak-over-threshold. *Comput.-Aided Civ. Infrastruct. Eng.* **2021**, *36*, 1150–1167.
73. Milani, A.E.; Antonello, F.; Baraldi, P.; Zio, E. A coevolutionary optimization approach with deep sparse autoencoder for the extraction of equipment degradation indicators. In Proceedings of the 30th European Safety and Reliability Conference, ESREL 2020 and 15th Probabilistic Safety Assessment and Management Conference, PSAM 2020, Venice, Italy, 1–5 November 2020. [CrossRef]
74. Galantucci, R.A.; Fatiguso, F. Advanced damage detection techniques in historical buildings using digital photogrammetry and 3D surface anlysis. *J. Cult. Herit.* **2019**, *36*, 51–62. [CrossRef]
75. Pierdicca, R.; Gorgoglione, L.; Martuscelli, M.; Usmanov, S. Challenging architectures: An integrated and multipurpose survey for the complete mapping of the emir palace in Kogon (Uzbekistan). In Proceedings of the 29th CIPA Symposium 'Documenting, Understanding, Preserving Cultural Heritage. Humanities and Digital Technologies for Shaping the Future, Florence, Italy, 25–30 June 2023; Copernicus GmbH: Göttingen, Germany, 2023; Volume XLVIII-M-2-2023, pp. 1225–1232.
76. Shanoer, M.M.; Abed, F.M. Evaluate 3D Laser Point Clouds Registration for Cultural Heritage Documentation. *Egypt. J. Remote Sens. Space Sci.* **2018**, *21*, 295–304. [CrossRef]